11-3-2016

Corrosion Characteristics of Magnesium under Varying Surface Roughness Conditions

Yahya Efe Yayoglu

University of South Florida, efeyayoglu@gmail.com

Corrosion Characteristics of Magnesium under Varying Surface Roughness Conditions

by

Yahya Efe Yayoglu

A thesis submitted in partial fulfillment
of the requirements for the degree of
Master of Science in Mechanical Engineering
Department of Mechanical Engineering
College of Engineering
University of South Florida

Major Professor: Nathan B. Crane, Ph.D.
Nathan D. Gallant, Ph.D.
Ryan Toomey, Ph.D.

Date of Approval:
October 25, 2016

Keywords: etching, medical, sbf, contact angle, Cytop, stearic acid, wetting, hydrophobic

DEDICATION

I dedicate this thesis to my parents. Thank you for your love and support throughout my life.

ACKNOWLEDGMENTS

TABLE OF CONTENTS

LIST OF TABLES

LIST OF FIGURES

iv

ABSTRACT

The biggest challenge with magnesium alloy biodegradable implants is the rapid corrosion at the earlier stages of the healing process after implantation. In this research, the impact of surface roughness generated by different means on the corrosion rate of AZ31 magnesium alloy in a simulated biologic environment is investigated. In order to perform accurate experimentation, an in vitro setup is assembled that simulates the human body environment accurately has been prepared using Schinhammer's in vitro immersion testing setup [1] and Kokubo's Simulated Body Fluid (SBF) [2]. For the immersion test of Mg in SBF, several surface texture groups of Mg have been prepared and submerged into the in vitro tank. The Mg samples' comparative analysis has been made in terms of corrosion rate, total weight loss and hydrogen gas evolution within a span of 7 days for the first experiment to narrow down the scope and 14 days for the follow up experiment. After 14 days of in vitro immersion test with varying roughness and hydrophobic modifications such as Cytop coating and stearic acid modification, it has been observed that the roughness group created by etching in aqueous NaCl solution for three minutes, shows better corrosion resistance compared to the polished control group. Hydrophobic modifications on the surfaces did not affect the corrosion behavior significantly.

CHAPTER 1: INTRODUCTION

1.1 Background on Magnesium in Medical Field

Medical applications have been positively affected by the implementation of the biodegradable materials since the ancient times starting with the Catgut sutures made out of sheep intestine [3] that dissolve in applied tissue after complete healing is achieved. Biodegradable materials used as temporary implants inside living subjects, eliminate the need for additional surgical removal operations by dissolving and joining the metabolism after remaining intact and keeping their physical properties until the connected tissue is healed completely [4, 5]. Since the ancient times up to modern day, biodegradable material technology improved significantly. Currently several biodegradable material alternatives are in use include but not limited to; iron (Fe), iron alloys and polymers like poly glycolic acid (PGA), polylactic acid (PLA), poly ε-caprolactone(PCL), poly ortho esters (POEs), poly 3-hydroxybutyrate (PHB), polyanhydrates, poly propylene fumarates (PPF), poly ethylene glycol (PEG), tyrosine derived polycarbonates [6]. Furthermore, ongoing researches on the topic are focused on allowing the use of several metals, alloys, composites and polymers which will provide wide selection of medical solutions for different situations that require diversified needs such as strength, lightweight, elasticity and porosity.

Today, one promising material that is being researched in biodegradable applications is magnesium. 70 years after its first production by Sir Humphry Davy in 1808, magnesium was documented to be used in the medical field for the first time as a ligature wire in pure form [7]. Following that breakthrough, along with its pure form, several different types of

1

magnesium alloys and treated magnesium have been serving the medical field. Magnesium is beneficial due to its biodegradability and relatively better mechanical properties such as low density and high strength compared to the alternatives like steel and aluminum [8, 9]. Potential applications of medical magnesium as biodegradable implants include cardiovascular stents, wires, connectors, musculoskeletal applications and sutures [7].

Along with the great benefits of magnesium implants, there are drawbacks that require further research and improvement in order to render effective implant solutions using magnesium. Magnesium oxidizes and dissolves over time within the body environment. During and after the oxidation, the resultant magnesium ions can be resorbed within the body to join and support the bone tissue [10]. The total corrosion reaction of magnesium in fluid environment is stated with the following formula [11, 12]:

$$Mg + 2H_2O \rightarrow Mg(OH)_2 + H_2$$ Equation 1

The major issue with implanted magnesium degradation is the rapidness of corrosion and the evolved hydrogen gas that comes with it. Lespinasse indicated that at 0°C temperature for 24 milligrams of pure magnesium, 22.4 cm^3 of hydrogen is generated which translates to the fact that within the warmer body environment each milligram of magnesium will liberate 1 cm^3 of hydrogen gas [13]. Even though moderate hydrogen gas evolution is tolerable within the body by absorption of the gas up to a certain rate [14], rapid hydrogen evolution in body environment results in undesirable situations such as internal gas bubbles under the skin around the healing area [15]. Additionally, the implant may lose its mechanical integrity prematurely due to fast corrosion before the tissue healing is complete. This phenomenon sums up the major obstacle that keeps the applications of

2

biodegradable implants made out of magnesium and its alloys below a certain level, especially for the relatively large volume orthopedic implant applications.

In order to resolve the rapid accumulation of hydrogen within the body, several studies are being performed. Most of the studies involve applying a certain corrosion resistive coating on the surface of the magnesium implant that will slow down the corrosion speed hence the hydrogen gas evolution rate [16]. With this research, an alternate solution is investigated. In preference to using a polymer interference between the body environment and the magnesium implant surface we will endeavor to trap a layer of hydrogen gas to serve as a buffer between the magnesium and the corrosive fluids to slow down the corrosion rate.

1.2 Thesis Objectives and Hypothesis

Dissimilar to the current ongoing researches focused on creating a polymer to coat the implants' surface to decelerate the corrosion, the objective of this research is to test whether slower Mg corrosion rates can be achieved by altering the surface texture of Mg plates. The optimal surface texture will entrap hydrogen gas within the surface features, hence create a hydrogen gas layer over the surface, evolved from the oxidizing Mg itself (Figure 1.1). This surface texture should be easily applied to complex surfaces used in medical devices.
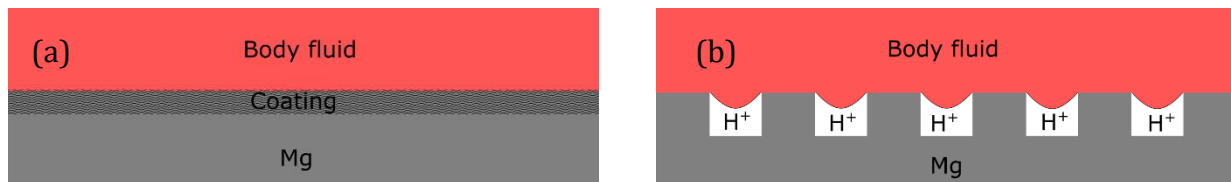
Figure 1.1: Not to scale illustration of (a) polymer coating method (b) bubble entrapment hypothesis to slow down the corrosion.

Even though several studies have been performed on surface wettability of magnesium substrates [17-21] this research is mainly focused on the modified surfaces'

corrosion behavior in an accurate in vitro setting. Also the methods to alter the surface characteristics were kept simple that enables the repeatability that reduces the possibility of inconsistencies in the case of a future mass production.

On Chapter 2, a comprehensive literature review is done on studies done on preventing high Mg corrosion speeds.

Chapter 3 is dedicated to explanation of the in vitro tank setup, simulated body environment control, fixtures, measurements done on the system, surface texture generation methods on Mg plates, effects of hydrophobic behavior on hydrogen gas entrapment along with the analytical data yielded from the preliminary immersion testing to narrow down the scope of the investigation on surface types.

The output data from the in vitro experimentation is processed and discussed in Chapter 4, and tied to a conclusion in Chapter 5.

CHAPTER 2: LITERATURE REVIEW

2.1 Factors that Influence Corrosion Rate of Magnesium

The main focus of this research is to investigate the surface geometry profiles' effect on the corrosion rate of H21 tempered AZ31 magnesium alloy. To have an idea of other factors that might influence the corrosion behavior of the samples, a review is conducted on the effects of alloying, coating and heat treatment.

2.1.1 Alloying

Magnesium has good mechanical properties such as high strength and low density which makes it desirable for the industry of aerospace and automotive. However the biggest problem is the high reactiveness of magnesium in corrosive environments and atmospheric air also. Corrosion resistance of magnesium is improvable by alloying with other less reactant (passive or inert) metals such as Ni, Ti, Al and Cr. However there is a challenge of keeping the high strength to weight ratio that magnesium offers. Since magnesium is highly chemically active, to compensate for the reactiveness, large portions of less reactant metals needed to be used in the alloy and this deteriorates the mechanical advantages [22].

On the other hand there is a possibility of a large tradeoff between corrosion rate and mechanical properties in biomedical applications unlike the aircraft and automotive industry which can't afford to have corrosion vulnerability. Song et al. [22] mentions the need of high ratio of non-reactant metals is needed in the Mg alloy to have inert overall corrosion properties. In biomedical applications the alloy does not needed to be highly inert, as it is desirable to degrade over time. Hence it is possible to have improved corrosion

5

resistance up to a certain level by still keeping good mechanical properties for biomedical applications with using low percentages (<5%) of alloying metals.

The use of rare earth elements in magnesium alloys for biodegradable implant applications is fairly common. Even though rare earth elements are highly reactive by themselves, in compound form with other noble elements such as Al, Mn, Zn, Fe, Cu and Ni their corrosion characteristics are stable due to the compounds' low electrode potentials hence those compounds are good candidates to be alloyed with magnesium to lower the overall corrosion response. There are 17 rare earth elements that include scandium, yttrium, and lanthanum which are the most common ones used in alloying. Those 17 elements are divided into two groups named as cerium and yttrium groups. Cerium group is composed of light rare elements and yttrium group is relatively heavier. Overall it is possible to create alloys with improved mechanical and anticorrosion properties such as WE43 magnesium alloy which is a rare earth element alloy consists of yttrium (RE) compound with zirconium [23].

Chen et al. compared the biocompatibility and biodegradability properties of Mg-Zn alloys to PLLA which is a polymer that is also widely used in biodegradable applications. Materials' in vivo degradation comparisons showed that Mg-Zn alloy degraded faster with improved bone formation around the material compared to the PLLA polymer. This proves the inclusion of Zn in Mg alloys promote biodegradability while still keeping the implant biocompatible since both Mg an Zn can join bio-metabolism without causing any toxicity effects. Inclusion of Zn also relatively slows down the corrosion rates relative to high purity magnesium. It was observed that on Mg-Zn alloy, cell attachments were also superior to PLLA as a result of animal testing which is desirable for biocompatibility [24].

6

2.1.2 Coating

Magnesium coating technologies to bring down the corrosion rate include; electrochemical plating, conversion coatings, hydride coating, anodizing, gas phase deposition, laser surface alloying/cladding, organic/polymer coatings [25]. Gray et al. reviewed these several types of coating methods applied on magnesium for use of large scaled implementations like automotive and aerospace applications. However since the Gray's review paper does not include coating methods applied for biomedical applications, the details of large scale application specific methods are not included in this review.

When it comes to coating types that is used for biomedical / biodegradable applications of magnesium, there is a lack of scientific sources in literature since it is a relatively new area of interest and there are several currently ongoing researches related to it. Once the studies are complete and patents on coating alternatives are secured, scientific documentations are expected to increase in number [26]. So far today, Ca-phosphate and hydroxyapatite coatings' performance in biologic medium have been investigated in literature.

Waterman et al. [21] have investigated the effects of calcium phosphate coatings on pure magnesium for biomedical applications. The coating is applied in two steps. First, 15 x 15 mm squares of pure magnesium were electroplated in a 2M $Ca(NO_3)_2$ solution with a Pt plate as counter electrode. Samples were plated under 3.2V of voltage for 10 minutes resulting with a coating layer of calcium hydroxide ($Ca(OH)_2$). Subsequently as a second coating step, electroplated (ECAD) samples were coated with biomimetic method which involves dipping the ECAD samples into a high concentration (5x) SBF solution at 37°C and pH 6 (achieved by diffusing CO_2 gas into the SBF once before the experiment). The immersion

7

resulted in a CaP (calcium phosphate) coating on top of the ECAD calcium hydroxide coating. The reasoning behind the selection of SBF immersion for coating was explained with the method being a non-toxic and biocompatible method that does not involve any chemicals that is not present in a living body. Finally the corrosion resistance of uncoated, biomimetic coated and ECAD + biomimetic coated samples were tested in a Hank's balanced salt solution (HBSS) at 37°C and pH of 7.4 buffered with 25mM HEPES acid. Hydrogen evolution was observed over the course of 14 days. ECAD + biomimetic coated samples have shown the most resistance to corrosion. The comparison between three sample groups' corrosion amounts at the end of 14 days can be seen below.

Table 2.1: Comparison of hydrogen volumes [21].

Sample	H_2 at 14 days
ECAD + biomimetic	2.9 mL
Biomimetic	23.9 mL
Uncoated	35.6 mL

The superior corrosion resistance of ECAD coated samples is tied to the self-healing properties of the calcium hydroxide sub-layer where it fills in the eroded layers of the top CaP layer with calcium as it wears out [21].

Dunne et al. [27] studied the corrosion behavior of hydroxyapatite coated magnesium alloys. Hydroxyapatite is known for its biocompatibility. Blast coating deposition method has been used to coat three types of alloys (WE43, EW62, EW10X04) since conventional high temperature techniques is not compatible with magnesium due to its low melting temperature of 600°C. Spraying was done with a jet pressure of 0.55 MPa 50 mm above the alloy surface at ambient temperature. The resultant surface roughness (R_a) after the spray coating was higher (~1.6 μm) than the uncoated specimens (~0.5 μm). In vitro immersion test was conducted to compare corrosion behaviors of the coated and uncoated specimens.

PBS (Phosphate buffered saline) solution was used as a medium and samples were immersed for 10 days at 37°C temperature. Evolved hydrogen data yielded the data below. It was observed that EW62 alloy (6.03wt% Nd, 0.42 wt% Zr, 1.95wt% Y) with hydroxyapatite coating had the highest resistance to corrosion followed by the uncoated EW62. This also proves the importance of alloying in corrosion behavior. EW62 and EW10X04 are fairly new developed alloys that has shown good corrosion resistance relative to the conventional WE43 biodegradable magnesium alloy.
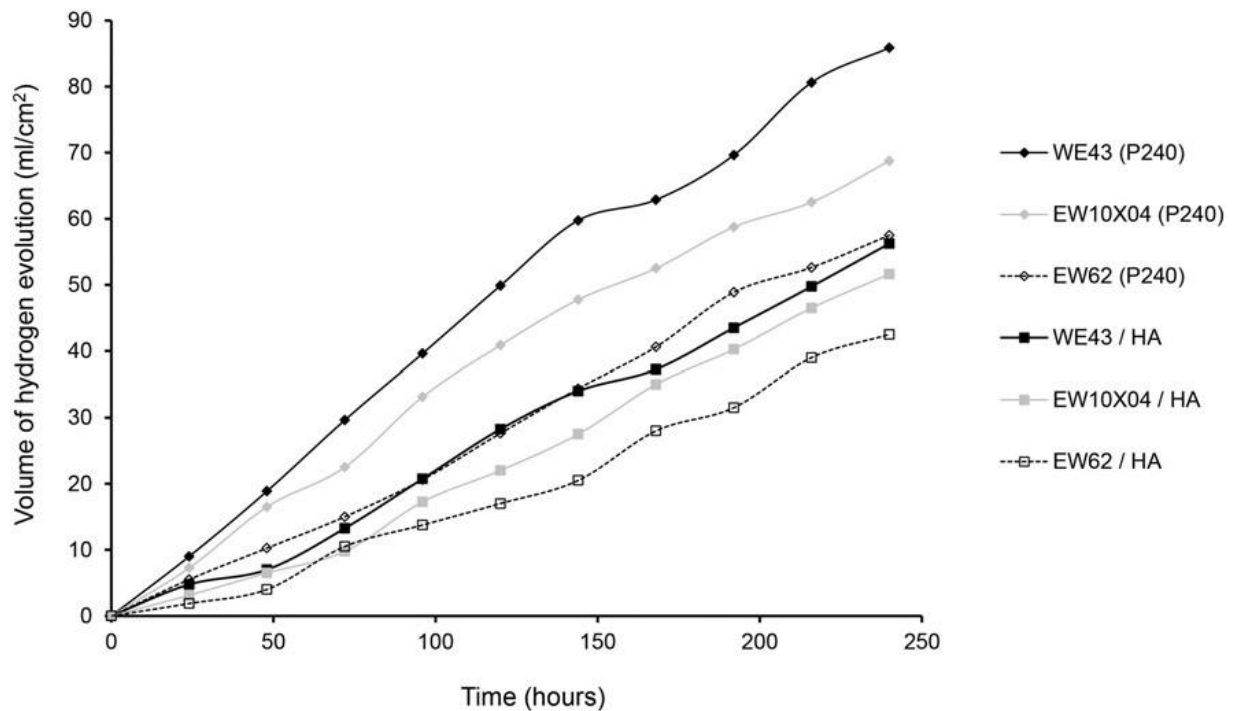
Figure 2.1: Evolved hydrogen volume in PBS solution. [27]

2.1.3 Heat Treatment

Another area of interest on corrosion resistance of magnesium and its alloys is heat treatment. Li et al. [28] investigated the "effect of heat treatment on corrosion behavior of AZ63 magnesium alloy in 3.5 wt% sodium chloride solution". To observe the corrosion rate, gas collection method is used by placing funnels above the samples and trapping the evolved gas during corrosion. The samples were prepared starting by manual alloying of AZ63 by

9

melting pure metal ingots of Mg, Al, Zn an Mn together in a furnace at 720°C, then pouring them into a preheated steel mold resulting a solid AZ63 alloy with composition of 5.7 wt% Al, 2.7 wt% Zn and 0.3 wt% Mn with remainder Mg. After pouring into the mold, the alloy is cooled by water. Subsequently one group was heated up to 385°C and quenched in water for 20 hours (referred as homogenized group - T4) while another group was heated up to 260°C and quenched in water for four hours (referred as peak aged group - T5). Untreated as cast samples corroded more slowly than both T4 and T5 samples (Figure 2.2) which correlates with the statement of Wang et al. [29] that claims precipitates existing within the alloy decreases the corrosion rate.
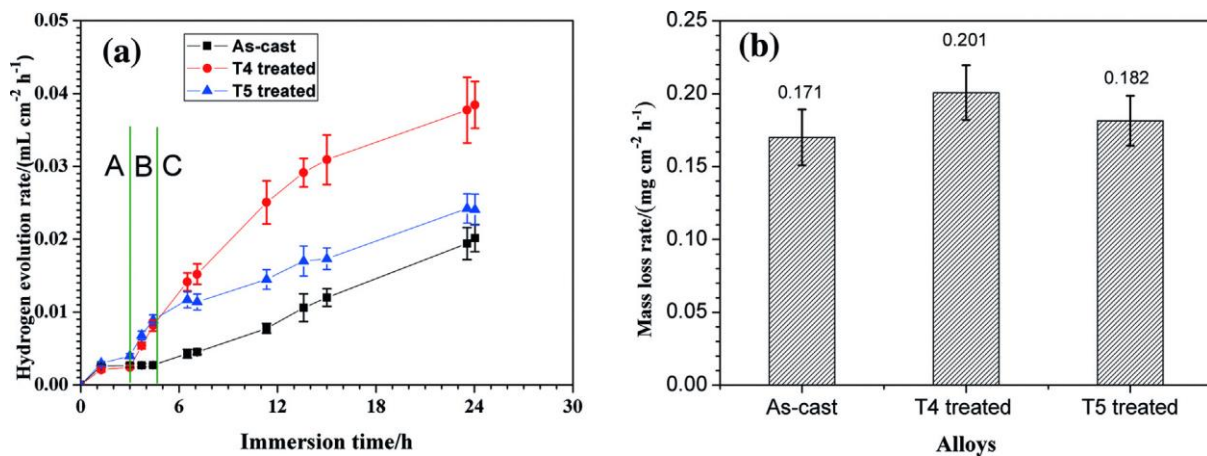
Figure 2.2: (a) Evolved hydrogen and (b) mass loss in NaCl solution for different heat treated samples. [28]

2.2 Wetting Behavior and Corrosion Resistance Relation

Wang et al. [18] worked on a similar hydrophobic surface generation method similar to the method applied on copper. An AZ91D magnesium alloy was used as a substrate and etched in an optimal SCE solution (containing 50 mLL^{-1} Ch$_3$COOH. 15 mLL^{-1} 85wt% H$_3$PO$_4$ and 5 mLL^{-1} 65wt% HNO$_3$). Then, subsequently etched samples were dipped in a solution containing 120 gL^{-1} Na$_2$P$_2$O$_7$10H$_2$O, 30 gL^{-1} ZnSO$_4$7H$_2$O and 5 gL^{-1} Na$_2$CO$_3$ at 80°C resulting in a Zn coating over the etched surface. Finally after forming the microstructure with etching

10

and zinc deposition, the surface was modified with stearic acid. Stearic acid modification was done with 0.01 molL-1 ethanolic stearic acid solution that contains 0.1 gL-1 sodium acetate to improve electrical conduction since 15 V of voltage was applied during the stearic acid immersion. Those processes resulted in a superhydrophobic surface on the magnesium alloy. On top of that, improved corrosion resistance due to super hydrophobicity was measured by immersing the prepared samples into 3.5wt% aqueous NaCl corrosive medium. Hydrophobic surfaced samples showed hardly any damage due to corrosion on the surface after 24 hours of immersion while unmodified samples were severely eroded after only three hours. The mechanism behind the anti-corrosion behavior of hydrophobic surfaces is explained by the trapped air between the medium and the surface (see Figure 2.3).
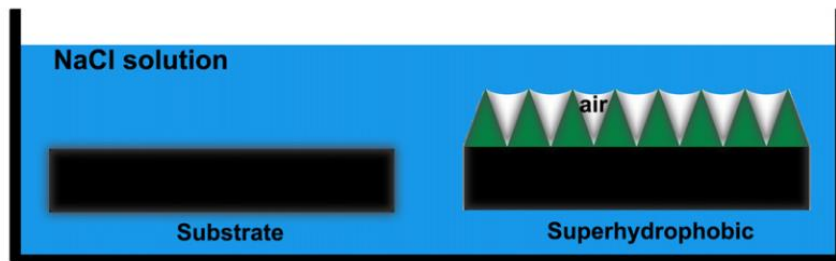
Figure 2.3: Anti corrosion mechanism of superhydrophobic surfaces. [18]

Additionally Wang et al. introduced another method to measure the hydrophobicity levels by sticking and adhesive tape on the surfaces and measuring the delamination due to the adhesiveness of the surface. Adhesive behavior is expected to decrease with increasing hydrophobic behavior, which was the case for their experiment.

2.2.1 Alternative Methods to Decrease Wetting Behavior on Solid Surfaces

Zhao et al. investigated ways of creating superhydrophobic textures by generating highly uniform pillar geometries on a solid surface. Silicon wafers were used as a substrate and dense pillared structures with 7 μm height and 2.7 μm diameter were created with the

11

help of a photo resistive polymer and etching away the exposed areas with an etching agent. The resultant geometry yielded a superhydrophobic behavior without applying any coating which is an interesting improvement area that could be applied on metals [30].
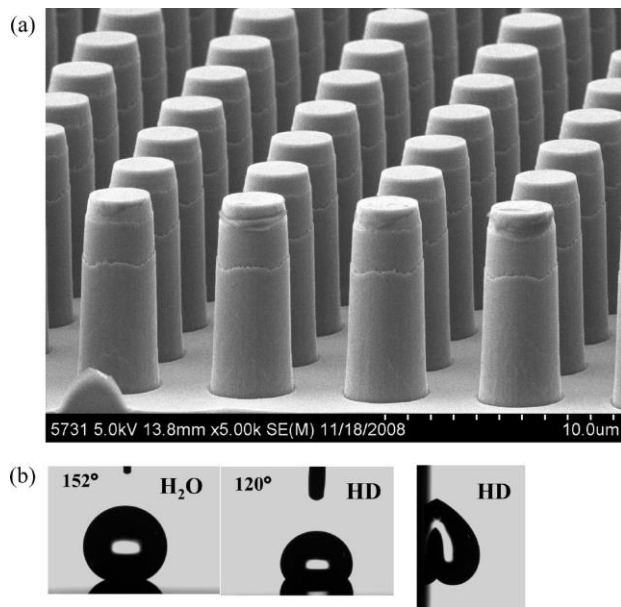
Figure 2.4: (a) SEM imagery of textured Si surface (b) Contact and sliding angle measurements. [30]
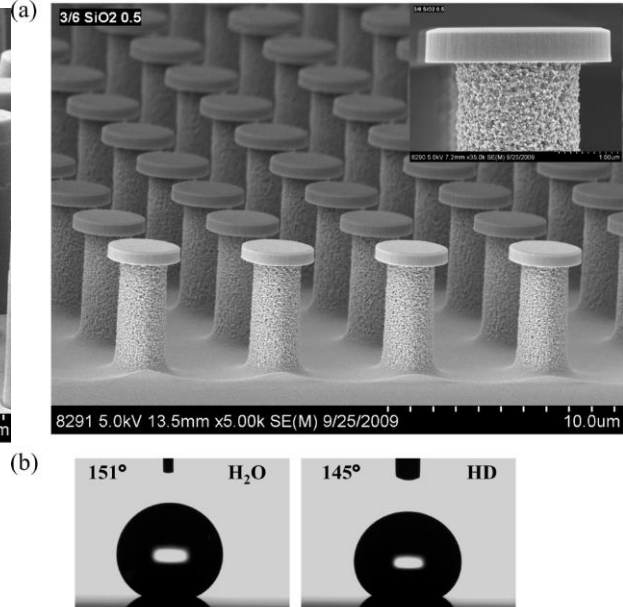
Figure 2.5: (a) SEM imagery of textured Si surface (b) Contact and sliding angle measurements. [30]

Wang et al. investigated a two-step approach to generate superhydrophobic surfaces on copper. Copper foils were first dipped into a 30% and 20% volume fraction antiformin solutions with varying durations between 15 seconds and 20 minutes. The effect of volume fraction and immersion duration is observed with the trial of different volume fractions and durations. The resultant structure formed on the copper substrate was in the form of micro wires forming a thin CuO film over the surface. It was observed that with immersions durations higher than 2 minutes in 30% VF antiformin solution, thin wire structures started to coagulate and form bean sprout-like structures on the surface. All samples immersed in antiformin solution regardless of time and solution concentration have shown superhydrophilic behavior with contact angles lower than 8 degrees. Following the

12

antiformin dipping, the samples were modified in 0.01 M ethanolic stearic acid solution for 15 minutes to lower the surface energy. With the stearic acid modification, all samples regardless of the immersion time and antiformin concentration, have shown superhydrophobic behavior with contact angles higher than 155 degrees. Wang demonstrated a time-saving, practical, and pollution friendly method to generate a superhydrophobic coating on a metal substrate [17].

2.3 In Vitro Testing Methods

An earlier study done on 2005 by Witte et al. [31] has investigated the correlation of in vivo and in vitro corrosion measurements. Immersion tests were conducted using AZ91D and LAE442 alloys along with in vivo experiments in animal tissue. The resultant corrosion characteristics did not correlate between in vivo and vitro setups. However the in vitro setup environment used to simulate bio organism was based on ASTM-D1141-98 protocol which is a substitute for ocean water instead of a biological fluid. Hence it was expected to observe a lack of correlation. Systems that simulate a biological environment more accurately were introduced later on with the adoption of SBF (simulated body fluid) and control systems that regulate pH and temperature that became more and more commercially available in time like Schinhammer's setup explained below.

Schinhammer et al. have introduced a fully automated in vitro setup that simulates the body environment implementing the SBF solution. The system consists of temperature and pH regulation with the use of CO_2 diffusion into the in vitro tank instead of using the traditional pH buffering methods such as using Tris, PBS or α-MEM buffered SBF solutions as medium. Their tests with WZ21 magnesium implant alloy have shown a corrosion behavior very similar to an in vivo testing, which proves that CO_2 infused pH buffering is the

closest possible testing method to animal testing also given the fact that it is the same buffering system present in human blood. The comparative corrosion behaviors of WZ21 alloy in Tris, PBS, α-MEM and CO_2 buffered SBF solution along with in vivo testing can be seen below [1].

It should be noted that on PBS and Tris buffered systems the pH of the system is adjusted by dripping the corresponding buffering agents into the system which yields unstable pH characteristics between the intervened time points. Automated CO_2 buffering allowed precise pH regulation that is always kept within the tolerance limits (pH 7.40 ±0.05) [1].
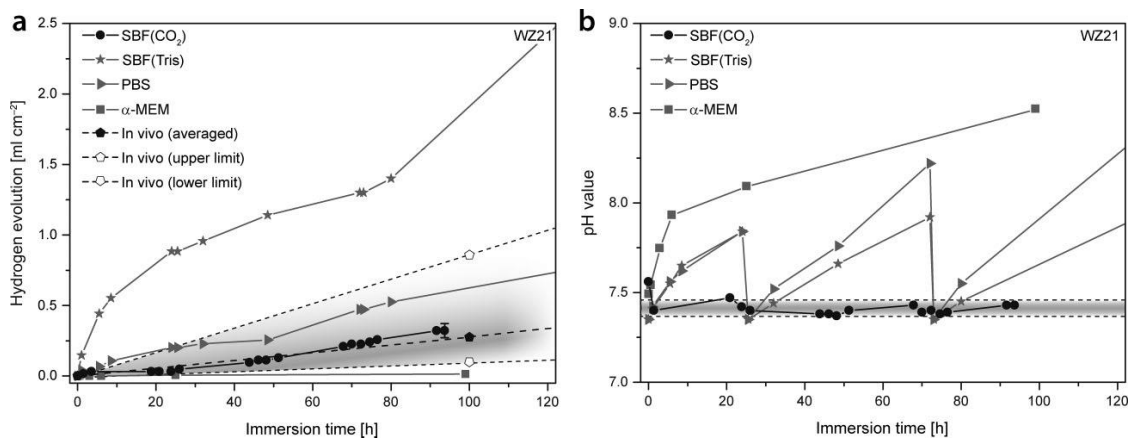
Figure 2.6: (a) Hydrogen volume evolution comparison of in vivo environment to various buffered in vitro setups (b) pH variance in differently pH regulated in vitro corrosive media over time. [1]

Wang and Li et al. For their immersion test in NaCl solution, the rates of corrosion in the corrosive medium was quantified by observing the pH change of the solution since the pH is expected to increase with the degradation of magnesium and release of hydrogen ions. Another measure of corrosion rate was to observe the concentration of dissolved Mg in the NaCl solution [18].

14

CHAPTER 3: EXPERIMENTATION

3.1 Introduction and Goals

The corrosion characteristics of magnesium with varying surface textures is observed using an in vitro experimental setup. Three main texture types including polished, micro roughness and macro roughness were generated for testing and selected texture groups were modified using a hydrophobic agent to observe the hydrophobic effect on corrosion resistance. The several texture types and their preparation methods are explained in depth on sections 3.3.3 through 3.4.2.2.

In vitro setup that simulates the body environment was the essential part of the study, since it is the closest possible experimental setup to animal experimentation (in vivo) that can be achieved in laboratory environment. In vitro experimentation will yield comparative evidence for the improved degradation behavior of modified magnesium surface within a biologic organism. The system is explained thoroughly on section 3.2. Promising treatment methods can then be investigated through "in vivo" testing.

Similar to the earlier studies conducted on effects of surface wettability on corrosion resistance reviewed on CHAPTER 2:, scientific proof of possible reduced corrosion behavior in simulated body environment by only altering the surface profile is one of the major goals of this research specific to biomedical applications.

3.2 In Vitro Test Setup

In vitro test setup consists of 20 liters of SBF (simulated body fluid) contained in a 10 gallon fish tank along with temperature and pH controlling unit (Arduino circuit). The generated magnesium samples with varying roughness were dipped into the SBF solution to see their corrosion characteristics in a simulated body environment. Special ABS sample holders that can hold 3 samples each were 3D printed. The holders that the samples were mounted on, are placed on a tray inside the SBF tank. The tray has 2.5 mm deep circular grooves with the exact diameters as the holders so that the holders can fit in tightly without floating. Magnesium samples are mounted on the holders using hot silicone glue (Ad tech Multi Temp) that also covers the side faces of the samples.

(a)
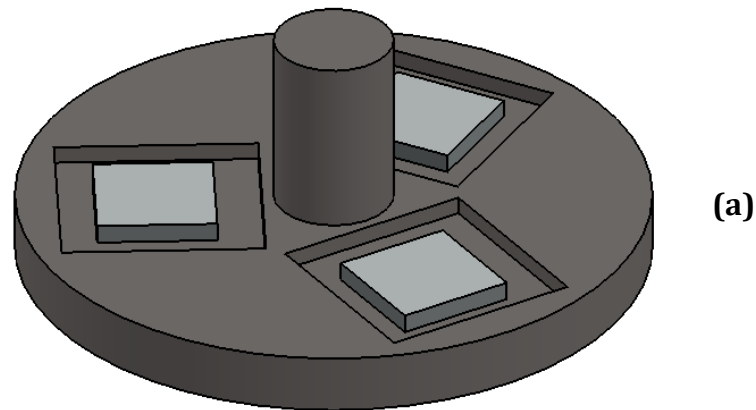
Figure 3.1: (a) Magnesium sample holder and (b) holder tray. (Dimensions are in mm)
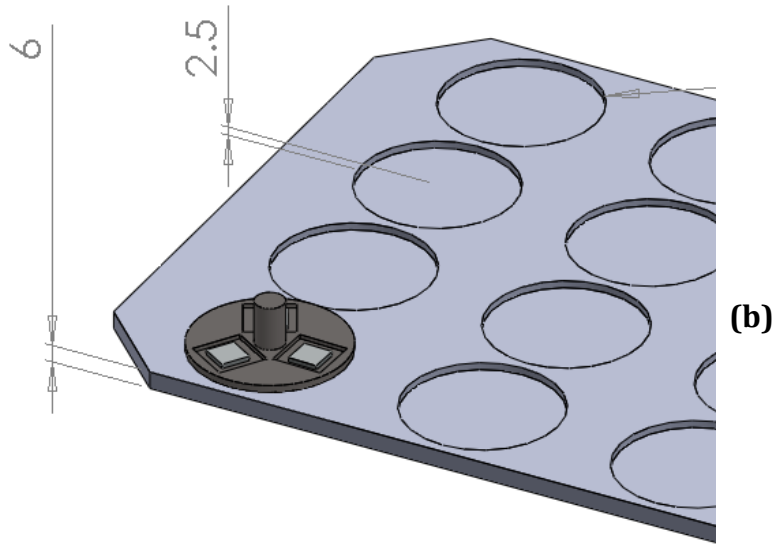
Figure 3.1 (Continued)

3.2.1 Simulated Body Fluid

The experimental procedure makes use of the Simulated Body Fluid (SBF) that has the same inorganic ion concentrations that is present within the extracellular fluid (blood plasma) of a human [2]. In preference to using the Kokubo's traditional recipe [2] for the SBF, Schinhammer's alternative body simulation method [1] was implemented. Schinhammer's method incorporates an automated carbonating system that adjusts the pH of the SBF with diffusing CO_2 gas into the solution eliminating the use of Hydrochloric Acid (HCl) and Tris ($C_4H_{11}NO_3$) as pH buffers. By implementing this method the HCl and Tris reagents were omitted from the traditional Kokubo recipe, yielding the SBF recipe that can be seen on Table 3.1.

17

Table 3.1: Reagents for preparation of un-buffered SBF (1L)

Order	Reagent	Amount
#0	De-ionized Water	1000 ml
#1	NaCl	7.996 g
#2	$NaHCO_3$	0.350 g
#3	KCl	0.224 g
#4	$K_2HPO_4.3H_2O$	0.228 g
#5	$MgCl_2.6H_2O$	0.305 g
#6	$CaCl_2$	0.278 g
#7	Na_2SO_4	0.071 g

20 liters of SBF is prepared in a previously sterilized 10 gallon transparent fish tank by adding reagents in the given order on Table 3.1 at 36.5°C temperature. Preparation procedure was done while a submersible pump is run to provide complete dissolution by circulating the water within the tank. Then, finally the pH level is adjusted using the automated carbonation system that is explained in detail in section 3.2.2.
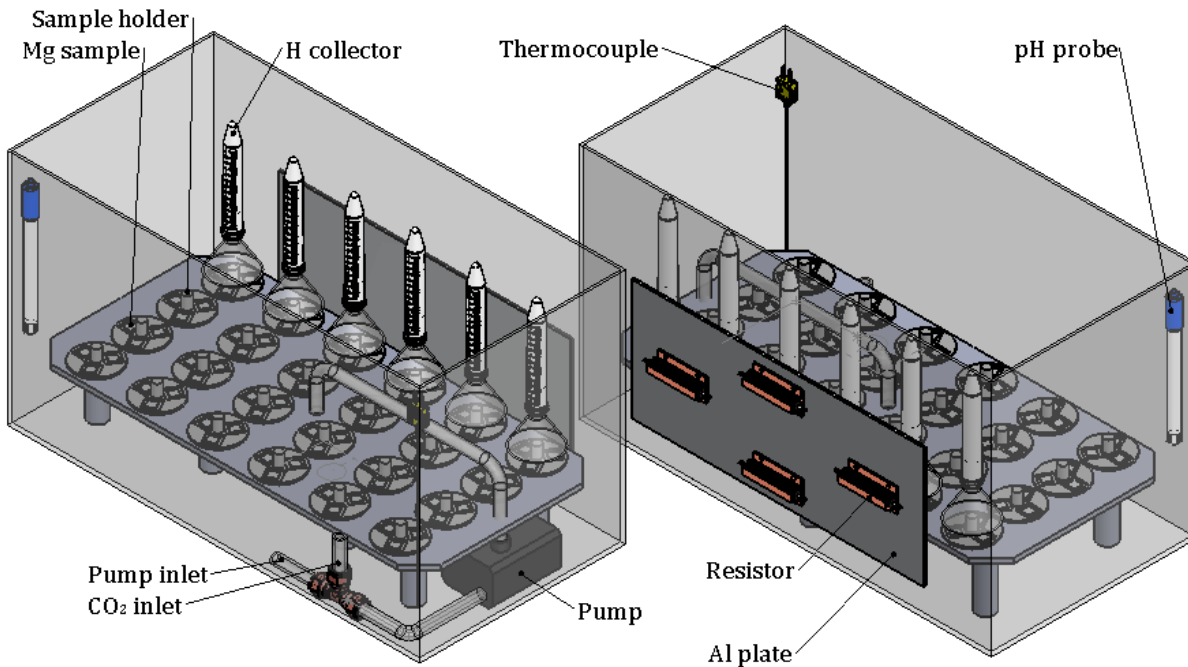
Figure 3.2: Front and rear view of the in vitro tank setup.

18

3.2.2 Temperature and pH Regulation

The temperature and pH regulation of the in vitro tank is done by a microcontroller implementation. The SBF needed to be kept at 36.5°C which is human body internal temperature and this is done by placing a custom made heat plate outside of the tank. 4 power resistors were connected together (see Figure 3.3) and mounted on an aluminum plate with 3 mm thickness resulting as an external heater with 360 watts of power. Heater is placed outside of the glass tank (Figure 3.2) by using thermal heat sink compound in between the glass and the metal plate.
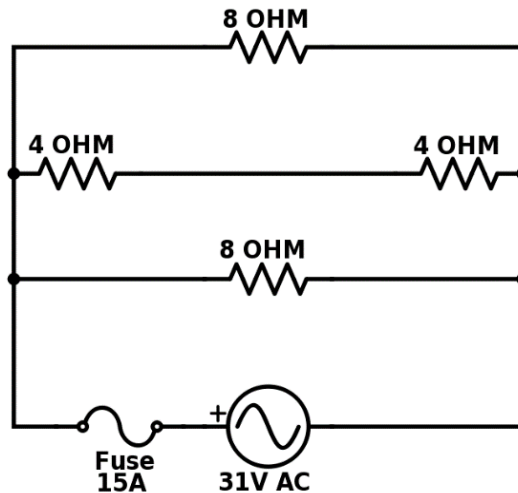
Figure 3.3: External tank heater circuit diagram.

Temperature feedback is done by submerging a K type thermocouple into the SBF solution. Thermocouple signal is sent to the Arduino microcontroller that determines when to switch on the relay that activates the 31V AC power supply. The relay is switched on when the temperature of the SBF is below the 36.5°C threshold. There was no need for a PID control since the system was overly damped and hard to overshoot the temperature value in a short period of time due to the large (20 liters) SBF volume.

19

As it has been indicated on section 3.2.1, pH is regulated by dissolving CO_2 gas into the simulated body fluid instead of using liquid pH buffers such as hydrochloric acid and tris. To do this, a pressurized CO_2 tank was used as gas supply and regulated using an electric solenoid valve integrated into the Arduino automation system. SBF's pH feedback to the microcontroller is done by using a pH probe (Gel filled glass, Beckman Coulter, U.S.A.) dipped into the tank. The detailed schematics of the pH and temperature control can be seen below on Figure 3.4.
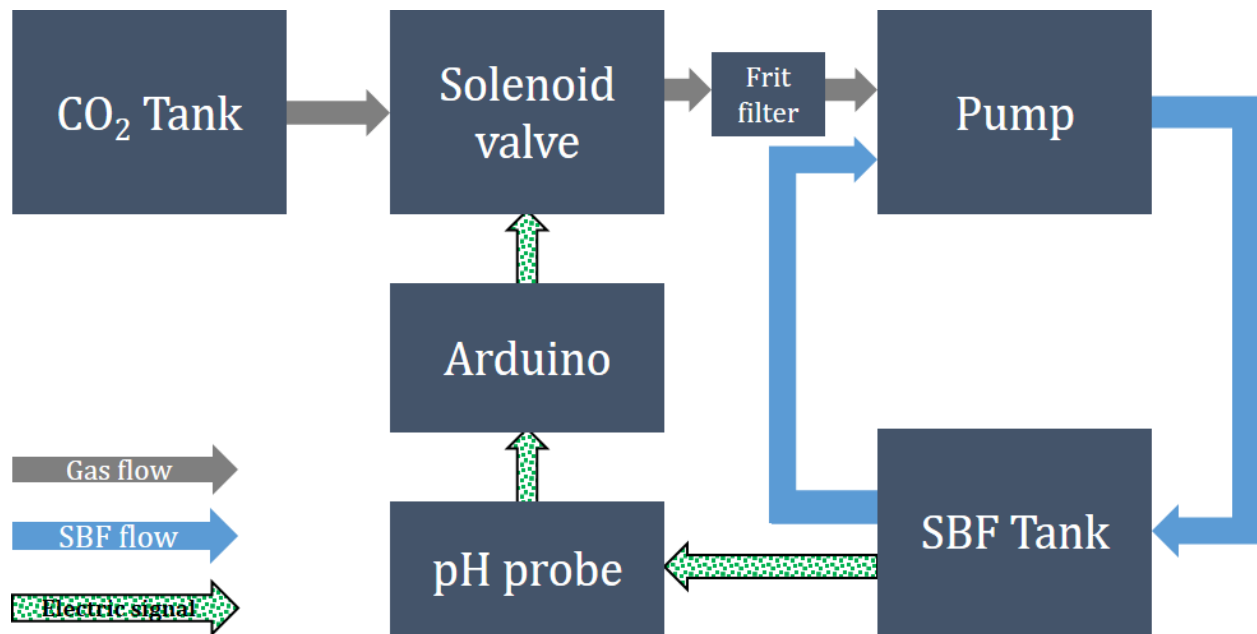
Figure 3.4: pH control setup illustration.

To ensure complete dissolution of CO_2 gas within the SBF, the gas enters the circulation after going through a frit filter with pores sized 2 µm. After the frit filter, the gas bubbles enter the pump where significant amount of circulatory movement happens, which improves the dissolution. At the outlet of the pump where SBF is released into the tank, there are almost no observable CO_2 bubbles, which is an indication of complete dissolution.

The temperature and pH values are logged into a spreadsheet file by the controller. This way it is ensured that the pH and temperature values are within boundaries all the time when the test setup is not under watch. Self-logging is helpful since the system is not under watch constantly within the duration of the experiments which can be as long as two weeks. Two immersion tests were run in the SBF tank for this research. First immersion test was for a time span of 7 days, and the second one was for 14 days. The pH and temperature readings for the duration of those two tests can be seen below.
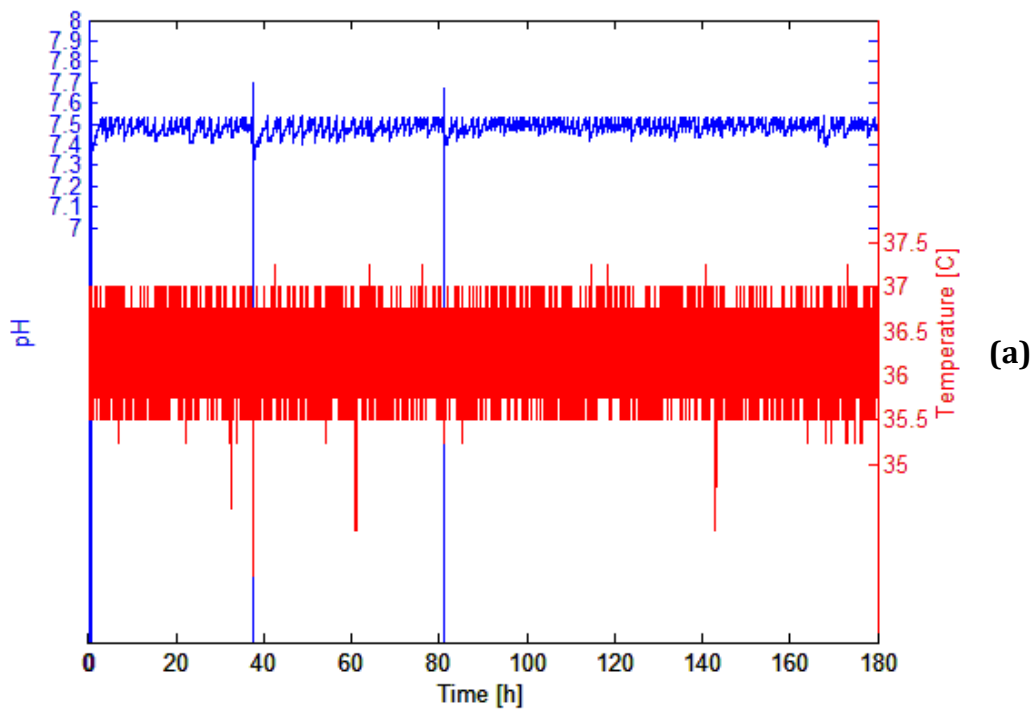
Figure 3.5: Temperature and pH log for SBF tank during (a) preliminary immersion test [7 days] and (b) follow up immersion test [14 days].

21
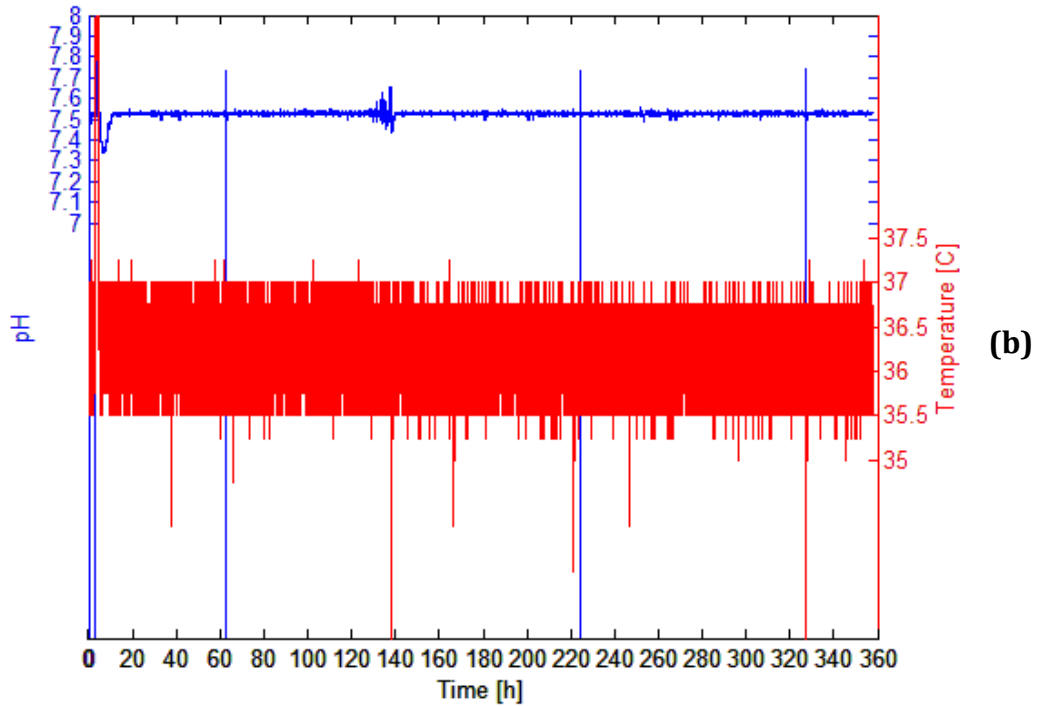
Figure 3.5 (Continued)

3.2.3 Data Collection

The corrosion rate of the samples is measured in two ways by measuring the mass loss before and after immersion and measuring the volume of liberated hydrogen during degradation in SBF. To measure the mass loss, samples were weighed on a precise calibrated scale and mass of each sample is recorded. Following the immersion testing, samples were chemically cleaned according to the ASTM G1-03 standard to remove the corrosion products off the surface then sonicated in DI water. After drying, the cleaned samples they were weighed to quantify the mass loss.

To capture the evolved hydrogen gas, funnels are used with graduated centrifuge tubes attached at the end (Figure 3.6). Funnels are placed above each specimen holder with the help of burette clamps. One extra capturing funnel was placed on a sample free region to ensure the funnels were only capturing evolved hydrogen due to corrosion.

22

The level of gas collected is noted on an average of daily intervals. Finally the captured hydrogen volume over time is converted to lost mass of magnesium with the method explained on the following section.
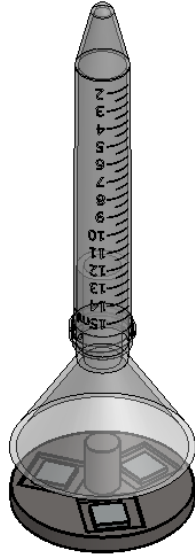
Figure 3.6: Hydrogen gas collector.

3.2.3.1 Hydrogen Evolution Method to Determine Corrosion Rate

In order to calculate the corrosion rate of magnesium specimens, evolved hydrogen volume and time points were taken as an input matrix and converted to corrosion rate matrix with the method explained below using the evolved hydrogen volume data for a test group.

$$Exposed\ surface\ area\ of\ Mg = A = 1\ cm^2$$

$$Inputs = \begin{bmatrix} 0 & Hydrogen\ Evolved\ (mL) & Time\ (h) \\ 31\ h & 0.35 & 31 \\ 53.5\ h & 0.40 & 22.5 \\ 78.5\ h & 0.50 & 25 \\ 124.5\ h & 1.00 & 46 \\ 148.5\ h & 1.10 & 24 \\ 171\ h & 1.40 & 22.5 \end{bmatrix} \qquad \text{Equation 2}$$

23

$$V_{hydrogen} = \begin{bmatrix} 0.35 \\ 0.05 \\ 0.10 \\ 0.50 \\ 0.10 \\ 0.30 \end{bmatrix} . mL \qquad time = \begin{bmatrix} 31 \\ 22.5 \\ 25 \\ 46 \\ 24 \\ 22.5 \end{bmatrix} . h. \frac{day}{24h}$$

Following calculations are done based on those evolved hydrogen volume ($V_{hydrogen}$) and time input matrices.

$$\dot{V}_{hydrogen} = \frac{V_{hydrogen}}{time} = \begin{bmatrix} 4.70 \; x \; 10^{-4} \\ 9.26 \; x \; 10^{-5} \\ 1.67 \; x \; 10^{-4} \\ 4.53 \; x \; 10^{-4} \\ 1.74 \; x \; 10^{-4} \\ 5.54 \; x \; 10^{-4} \end{bmatrix} . \frac{mL}{day} \qquad \text{Equation 3}$$

According to Lespinasse, 1 mg of corroded magnesium liberates 1 mL of hydrogen [13]. Validation of this approximation is derived on Appendix A using the same example values with stoichiometric approach.

$$\dot{V}_{hydrogen} = \dot{m}_{magnesium} \qquad \text{Equation 4}$$

$$\dot{m}_{magnesium} = \begin{bmatrix} 4.70 \; x \; 10^{-4} \\ 9.26 \; x \; 10^{-5} \\ 1.67 \; x \; 10^{-4} \\ 4.53 \; x \; 10^{-4} \\ 1.74 \; x \; 10^{-4} \\ 5.54 \; x \; 10^{-4} \end{bmatrix} . \frac{mg}{day}$$

Mass loss is defined as mass loss rate per unit surface area per time.

$$MassLoss = \frac{\dot{m}_{magnesium}}{A} = \begin{bmatrix} 4.70 \; x \; 10^{-7} \\ 9.26 \; x \; 10^{-8} \\ 1.67 \; x \; 10^{-7} \\ 4.53 \; x \; 10^{-7} \\ 1.74 \; x \; 10^{-7} \\ 5.54 \; x \; 10^{-7} \end{bmatrix} . \frac{g}{cm^2 . day} \qquad \text{Equation 5}$$

The corrosion rate (CR) equation is defined as the penetration depth over time in literature that has the unit of mm/day calculated by dividing mass loss by density of

24

magnesium which is 1.834 g/cm³. The final desired outputs of CR and time points for result discussion are obtained.

$$CR = \frac{MassLoss}{\rho_{magnesium}} = \begin{bmatrix} 2.56\ x\ 10^{-7} \\ 5.05\ x\ 10^{-8} \\ 9.13\ x\ 10^{-8} \\ 2.47\ x\ 10^{-7} \\ 9.51\ x\ 10^{-8} \\ 3.02\ x\ 10^{-7} \end{bmatrix} \cdot \frac{cm}{day} \quad Timepoints = \begin{bmatrix} 31 \\ 53.5 \\ 78.5 \\ 124.5 \\ 148.5 \\ 171 \end{bmatrix} \cdot h \quad \text{Equation 6}$$

3.2.3.2 Evolved Hydrogen and Mass Loss Correlation

For both immersion tests, hydrogen entrapment method was used to have complementary data to quantify corrosion rate besides measuring the mass loss only. To determine the accuracy of this method three identical test sample groups were prepared from polished, non-etched, non-modified samples. Samples were immersed into the SBF tank for seven days and evolved hydrogen due to corrosion was entrapped in the centrifuge tubes. The hydrogen volume levels are measured daily. Three sample groups were also placed separately on different locations of the tank to observe any location related effects that might distort the data like SBF circulation irregularities within the tank.

At the end of seven days after all corrosion products are removed off of the surface of the samples, total actual mass loss and theoretic mass loss calculated by Lespinasse's method (correspondence of 1 mL of evolved hydrogen to 1 mg of dissolved magnesium)[13] are compared. The correlation data can be seen below.
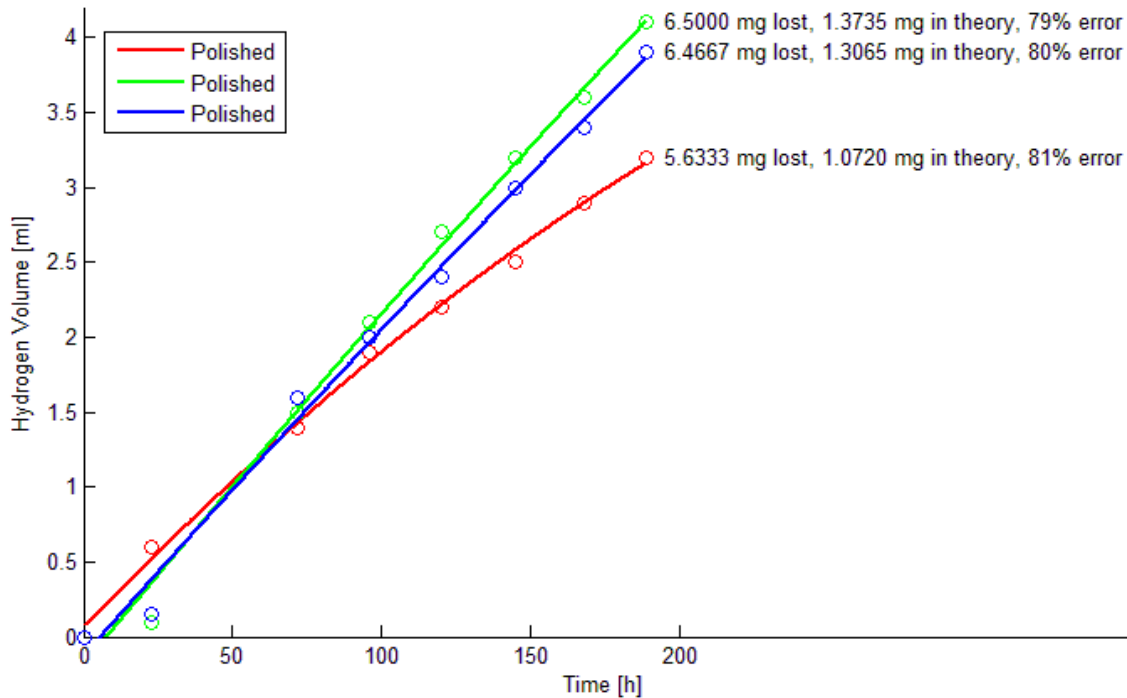
Figure 3.7: Captured hydrogen volume and mass loss correlation.

As a result of the data, it has been proven that the physical locations of the samples within the tank do not distort the data significantly. However, the conversion of captured hydrogen volume to theoretical mass loss, has shown that the use of hydrogen evolution method alone is not a useful tool to determine the lost mass since the actual mass loss measured by a scale before and after the immersion is off by 80% in average from the theoretical calculations. The reason behind this could be the lack of complete entrapment of hydrogen due to the spacing between the funnel and the sample holders, partial dissolution of hydrogen into the SBF, and diffusion of hydrogen out of the plastic funnel and centrifuge tube assembly. Despite those facts, hydrogen entrapment method may still provide a consistent comparative measure of corrosion speed since all of those handicaps are present for all samples within the test setup. In conclusion, hydrogen evolution method is kept as a comparative tool for corrosion speed but not used to determine mass loss.

26

3.2.3.3 Post Processing

After the samples are taken out of the SBF tank, to remove the corrosion products off the surface, they were cleaned in a boiling aqueous 15wt% chromium trioxide and 1wt% silver chromate solution for 1 minute specified in the ASTM G1-03 standard [32] to clean magnesium alloy corrosion test specimens. The effect of the cleaning process on the surface contamination levels can again be seen on Figure 3.23. After the cleaning process, samples are sonicated in DI water, then dried under vacuum at 100°C overnight.

To ensure the chemical cleaning process removes all of the corrosion products off the surface, the cleaning process was applied multiple times on a pre-immersed corroded test sample. After each cleaning, samples are dried and weighed. If some significant weight loss on the samples was observed between each cleaning, an additional cleaning cycle is performed and the process is repeated until the change is insignificant. After the third cleaning the weight loss dropped to zero for all samples which means no more corrosion products were left to remove from the surface. Also, to ensure the cleaning process was not etching away any of the actual magnesium, an un-modified polished sample was also cleaned at the same time with the test specimens as a reference. It has been observed that the weight loss on the reference sample was very insignificant after each cleaning step (See Table 3.2). In conclusion, cleaning the samples for three times was sufficient to remove all of the corrosion products without etching away the un-corroded magnesium itself.

Table 3.2: Mass loss of samples after each cleaning pass.

Sample Group	Avg. Mass Loss After First Cleaning	Avg. Mass Loss After Second Cleaning	Avg. Mass Loss After Third Cleaning
SBF Immersed (Corroded)	0.0035 g	0.0023 g	~0 g
Reference (No corrosion)	~0 g	0.0001 g	0.0001 g

After cleaning and drying process, samples were weighed to determine the mass loss caused by corrosion.

3.3 Preliminary Test Samples

3.3.1 Polished Surface (Base Samples)

In the preliminary tests, H24 tempered unpolished AZ31 magnesium alloy sheets that meet AMS QQ-M-44B specification with 1.6 mm thicknesses acquired from Small Parts, Inc. were cut into 15 x 15 mm squares using a hydraulic shear. Each individual square specimens were wet sanded with 600, 1200 grit sandpaper and 0.05 micron diamond polishing pad respectively using deionized water as coolant/lubrication. Back face of the samples were polished just with 600 grit paper to remove the default coating just enough to reveal the alloy to allow electrical conduction for future electro-etching applications. After each polishing cycle, specimens were immediately dipped into Ethanol to dissolve residual grease, then sonicated in de-ionized water to remove residual particulates and polishing media. Subsequently, each specimen is dried under a heat gun with moderate heat setting.

In order to have consistent exposed area for all test specimens, the edges and the back surface of all Mg squares that are sized approximately 15 x 15 mm were masked with corrosion protective stop-off lacquer (©Gesswein Canada, Part #210-1255) leaving an exposed area sized 10 x 10 mm (1 cm^2) exposed to the solution for testing (see Figure 3.9).

28

The precise deposition of lacquer on magnesium surface is done by deposition from a 3 ml syringe attached to a three axis CNC machine executing the first section of the G-Code on Appendix B. Flow rate of the lacquer from the syringe is adjusted manually by hand throughout the operation of CNC by adjusting the pressure within the cylinder that yields the desired flow rate. The pressure is adjusted once by pushing the plunger before the initiation of the g-code and once the flow rate reached to the desired level plunger is set free. Due to the short duration of the operation, the flow rate did not vary throughout the deposition process. Needle with 0.3 mm thickness is used for deposition.
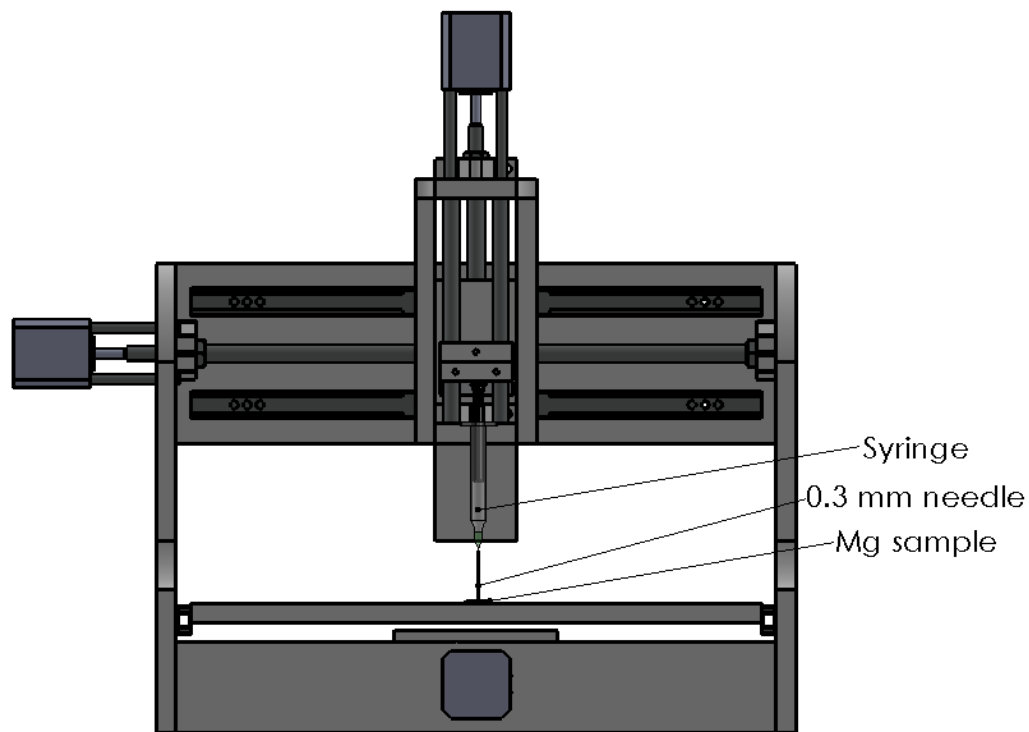
Figure 3.8: CNC lacquer deposition setup.

Remaining areas including the back surface that did not require precision deposition were coated with the same lacquer by hand using a thin brush. By the framing process, the

inaccuracies in exposed area dimensions due to imprecise hydraulic shear cutting of the samples were prevented.
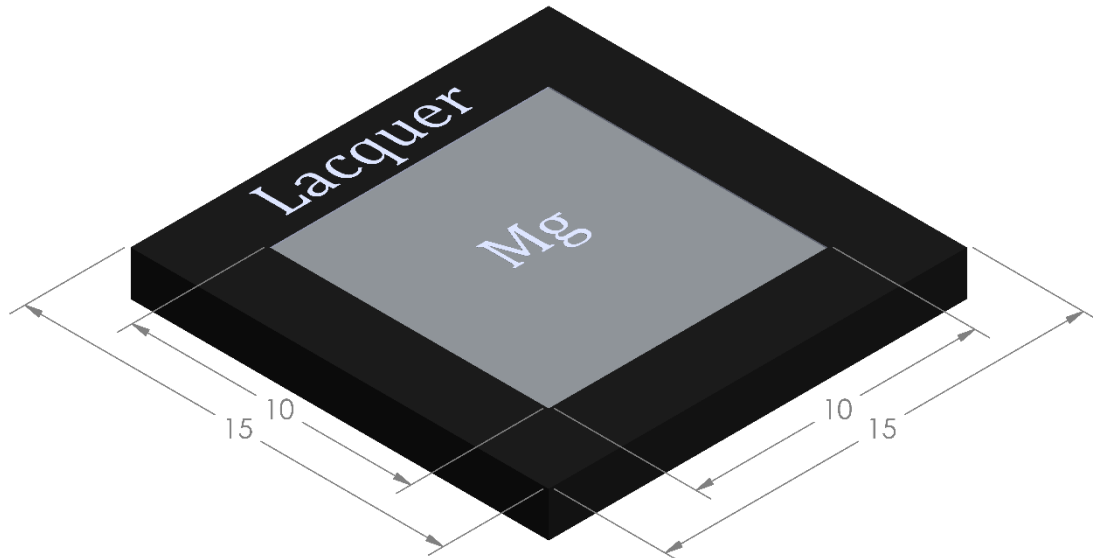
Figure 3.9: Base specimen dimensions in millimeters.

Polished specimens also form a base to all other texture types since they are all generated with additional applied processes that yielded the desired texture later on.

3.3.2 Macro Roughness

The purpose of the multiple roughness texture generation is to find the optimal roughness feature to capture hydrogen bubbles between the surface grooves. One candidate for that kind of texture is a short multi pillared structure that has small spacing between the pillars that is able to trap the bubbles after they are evolved during the corrosion process. However the dimensions of this pillar structure needed to be determined with several trials using different pillar sizes and spacing. Since the features of the roughness is easily visible to the naked eye, this surface roughness group is referred to as macro roughness group for ease of reference.

30

The first trial was done using the CNC needle deposition method that was also used to frame the polished base specimens. The prepared polished samples were deposited with the stop-off lacquer using the same CNC needle setup creating a dotted masking texture with dots approximately 0.6 mm diameter and 1 mm spacing in between (see Figure 3.10). After lacquer deposition the samples were left to dry for 2 hours, then dipped into 1M citric acid solution to etch away the un-masked areas for 3 minutes. The etching process yielded a short pillared structures. After etching, the samples were sonicated in acetone to remove the lacquer masking and then cleaned in DI water, finally dried under a heat gun in moderate setting. The lacquer frame around the edge that was removed during the acetone sonication is re-deposited with the CNC needle to re-achieve consistent exposed surface area.
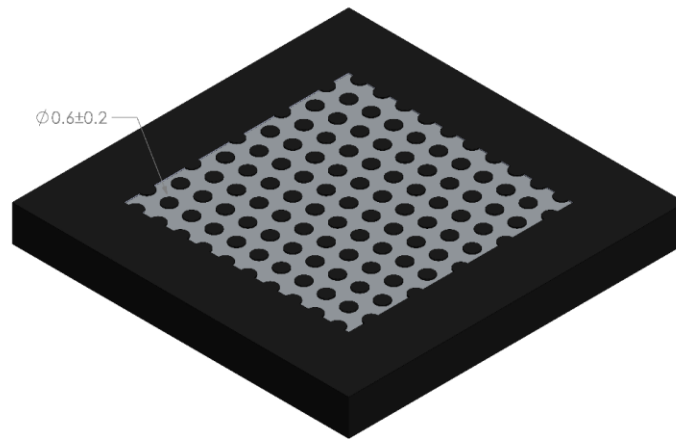
Figure 3.10: Representation of deposited lacquer using CNC syringe.

3.3.3 Micro Roughness

Third roughness group is generated using electro etching on the prepared polished specimens as mentioned in section 3.3.1. Since the finer shape profile cannot be observed by a naked eye, the specimen group is referred as micro roughness for ease of reference.

31
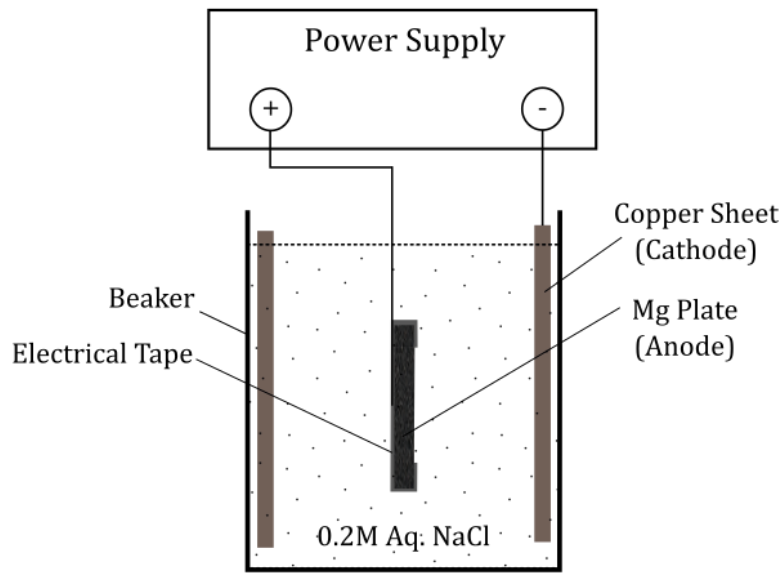
Figure 3.11: Cross sectional representation of the experimental setup.

The method to modify the surface roughness was picked such that incorporates commonly available materials and tools similar to Liang's research [19]. Polished specimens were etched in 0.2 mol/L aqueous NaCl solution in a 140 ml beaker, while applying electric current to create the electro-etching effect. A thin copper sheet is used as cathode and the Mg specimen is placed facing the copper sheet approximately 30 mm away from it (Figure 3.11). Large enough area is revealed by removing the stop-off lacquer on the back surface (to be recoated after the etching process) of the Mg specimen in order to allow electrical conduction. Wiring was attached to the mentioned lacquer-free region with the help of an adhesive copper tape.

The electro etching involves two process variables, which are; etching time and electric current. Those parameters needed to be determined beforehand through some preliminary testing by varying etch time and amperage separately and observing the effect.

32

The aim was to find the optimal etching time and current density that will yield the optimal roughness profile with minimal volume removal from the raw specimens by electro etching.

Additionally, the hydrophobic behavior of the etched surfaces with varying roughness is observed to have a reference point for further surface modifications on section 3.3.3.3.

3.3.3.1 Etching Time and Electric Current Density Influence on Roughness

Using the aforementioned electro etching setup, 15 samples were etched in 3 groups of 5 for 1, 3, 5, 7 and 9 minute duration. A current density of 100, 150 or 200 mA/cm^2 was applied to each of these three groups individually. Those current density values were picked within the output range of the power supply that has been used. Roughness of all samples were measured using a profilometer (Dektak 150 Surface Profiler) by scanning the surface on x, y and diagonal directions and taking the average of all passes for both arithmetic average and RMS roughness representations calculated using the formulas below [8]:

$$R_{avg} = \frac{1}{n}\sum_{i=1}^{n}|z_i| \qquad\qquad R_{rms} = \sqrt{\frac{1}{n}\sum_{i=1}^{n}z_i^2} \qquad\qquad \text{Equation 7}$$

The resultant roughness data with varying current density and etch duration can be seen on Figure 3.12.

33
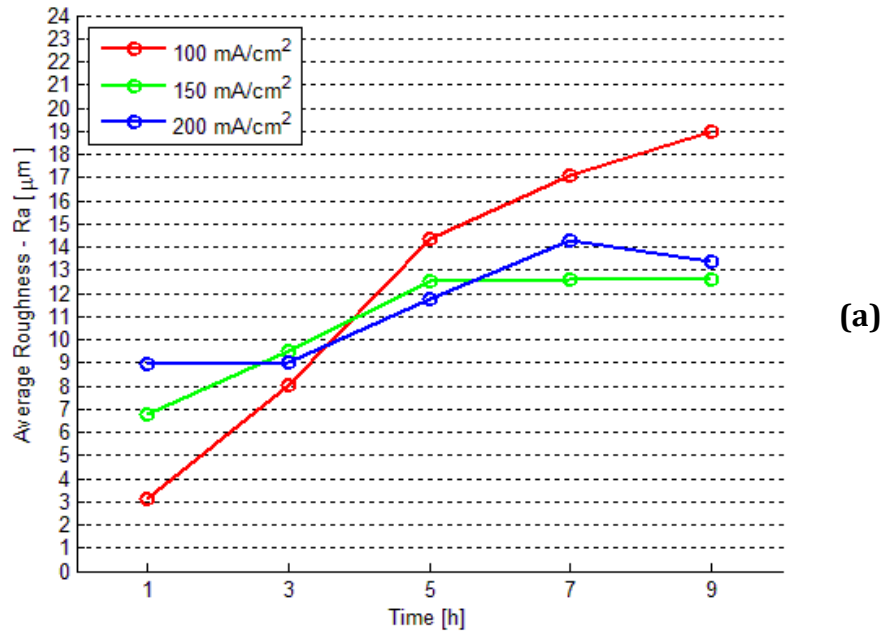
(a)
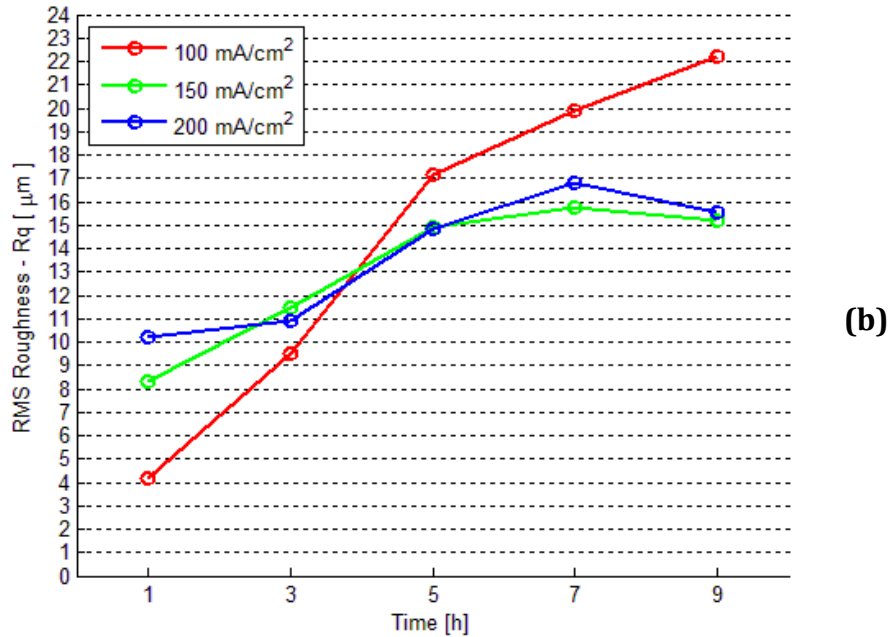
(b)

**Figure 3.12: Influence of etching time and current density on
(a) average roughness, (b) RMS roughness.**

It can be seen that with current density values higher than 100 mA.cm^{-2} the Mg

roughness does not increase, possibly caused by excessive erosion on the fine roughness

34

features due to relatively high current density. As a result, the optimal current density value was determined as 100 mA.cm^{-2} and the etch time was picked as 5 minutes to have an optimal roughness with minimal material removal off the polished surface. The etching depth and mass loss with increasing etching time data that yielded this conclusion is below. The etching depth is measured by masking a small area of a sample with etch resistant tape (electrical tape) during etching and measuring the resultant step height using profilometer.
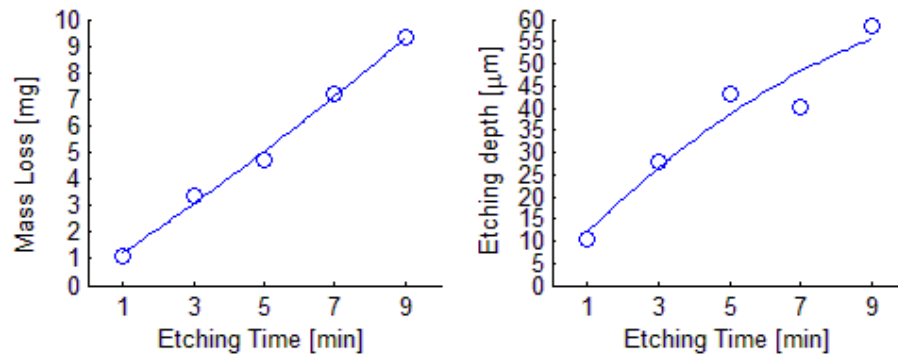
Figure 3.13: Mass loss and etching depth with increasing etch time.

On another note on Figure 3.12 it has been observed that, with increasing etch durations on lower current densities, the roughness also showed an increasing trend which means it might be possible to achieve greater roughness values with lower current densities or higher etch durations. This gained knowledge will be kept in consideration as an area of improvement for future research.

3.3.3.2 Roughness Influence on Hydrophobicity

Due to the positive correlation between hydrophobic behavior and corrosion resistance [18], contact angle measurements were taken on the etched samples.

To measure the contact angles droplet test is performed. 3 µL de-ionized water dropped on the surface and the contact angle images were captured by a camera (Edmund Optics, U.S.A.) using *uEye Cockpit* capturing software. Contact angles were measured for each

35

specimen using ImageJ 1.46r software with DropSnake plugin. The alignment to ensure levelness of the surface that the sample was placed on was done by overlapping a glass slide's front and rear faces' top edges on the camera view.
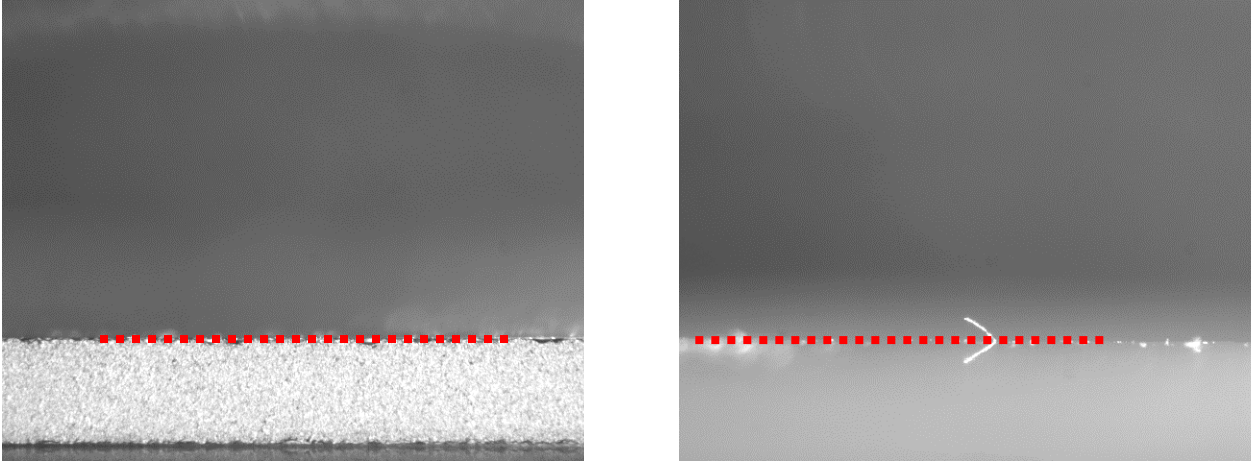
Figure 3.14: Contact angle measurement setup leveling by overlapping a glass slide's front edge (left) and rear edge (right).

Measurements were taken on each specimen 3 times and the average contact angle value is recorded. The resultant contact angle versus average and RMS roughness values are presented on Figure 3.15.

As expected, it is observed that hydrophobicity significantly decreased with increasing roughness without any further coating or modification. This is to be expected because roughness tends to increase both hydrophilic and hydrophobic tendencies of the base materials. However, hydrophobicity can be increased further by applying a thin hydrophobic coating. Additional modifications to achieve hydrophobic behavior, such as coating the surface with a hydrophobic agent is studied and discussed on the following section.
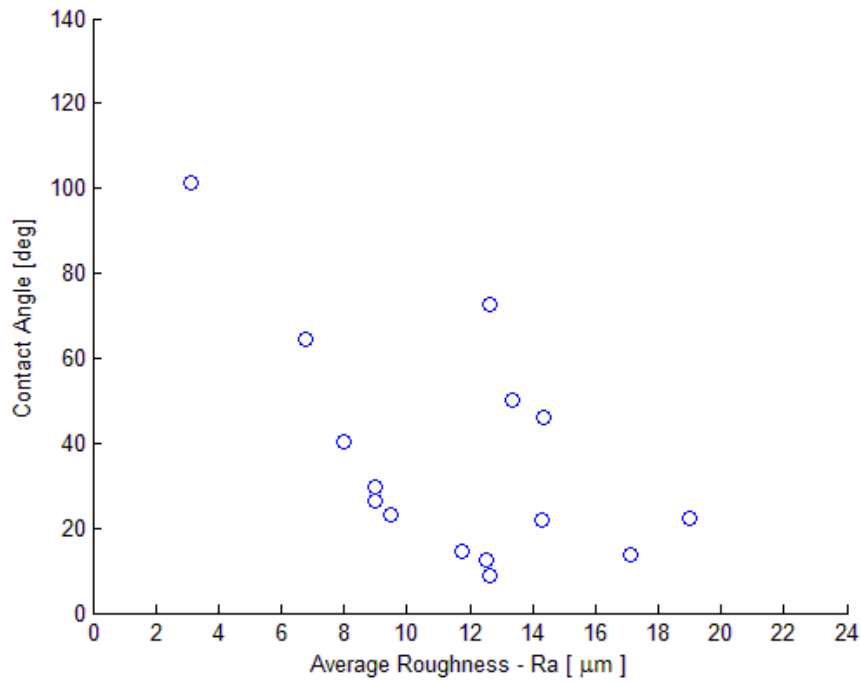
(a)
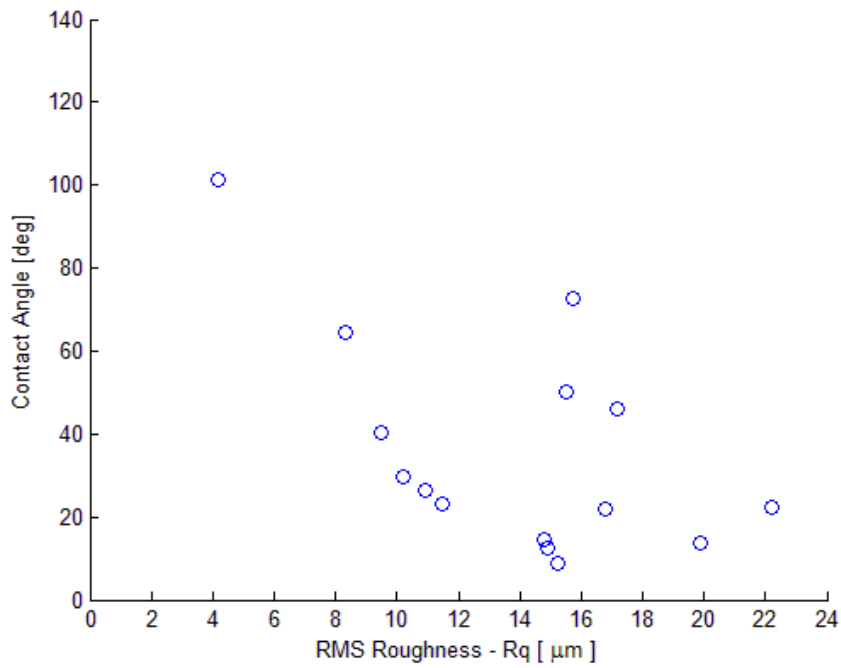
(b)

Figure 3.15: Variation of contact angle with (a) average and (b) RMS roughness respectively.

www.manaraa.com

3.3.3.3 Hydrophobic Coating Modification

Hydrophobic behavior will influence hydrogen bubble entrapment [33]. Wang et al. states that; as hydrophobic behavior increases, gas bubble entrapment between the micro level grooves will increase [18, 34].

While a treatment without any coatings would be ideal, the impact of hydrophobic coatings was included as it has a powerful impact on the surface wetting response of a textured surface. The rough surfaces with and without coatings were compared to assess the impact of the coating.

In order to achieve hydrophobic behavior, the etched specimens that were analyzed in section 3.3.3.1 were coated with a hydrophobic agent. The coating was done by dropping 9% diluted Cytop® (to dilute, solvent supplied with the Cytop agent is used) to the center of the square specimens and spinning them at 500 rpm speed for 10 seconds, then at 2000 rpm for 40 seconds to achieve uniform coating thickness over the surface. Following spinning, samples are soft baked in a furnace for 90 seconds at 90°C temperature, then hard baked for 30 minutes at 180°C. The resultant Cytop layer thickness was measured as 896 nm after the process. The thickness measurements were taken on a silicon wafer coated with the same spin method. Since the surface of the polished magnesium alloy was too rough / not reflective enough for accurate reflectometer (Filmetrics F20, U.S.A.) measurements.

The effect of etch time and current density on hydrophobic behavior is also observed on Figure 3.16 as complementary data to the determined etching parameters in section 3.3.3.1. It again has been shown that 5 minutes of etch time with 100 mA.cm^{-2} current density are the optimal parameters for etching to generate the micro roughness and the hydrophobic

macro roughness sample groups since after five minutes the roughness values started to plateau while the removed material still increased which was not desirable.
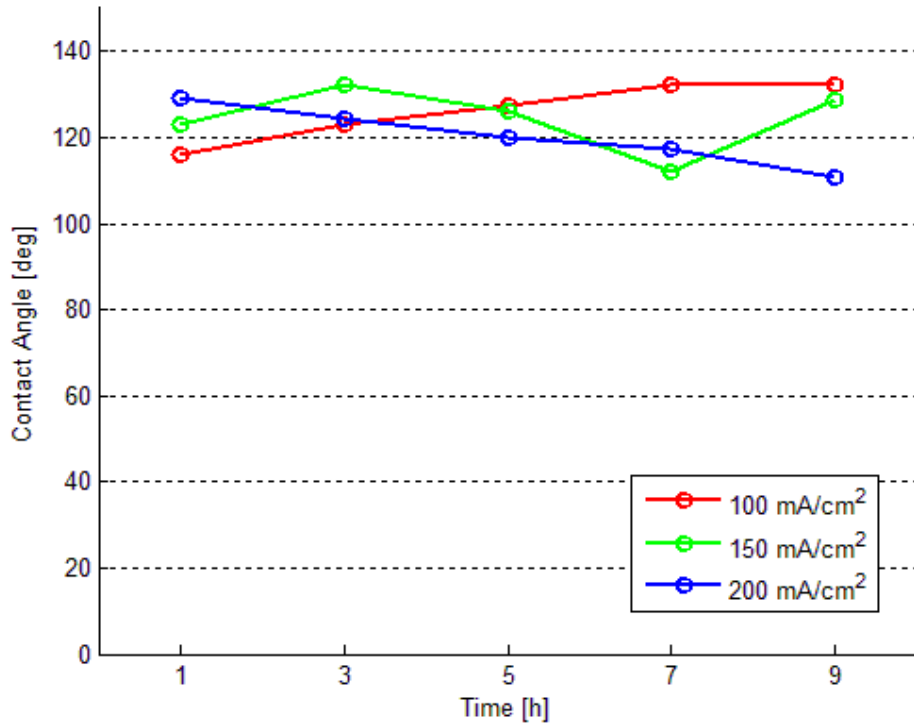
Figure 3.16: Influence of etching time and current density on hydrophobic behavior on samples with Cytop coating.

The effect of hydrophobicity with varying RMS and arithmetic average roughness values was again observed with the help of contact angle measurements. The influence of roughness on hydrophobicity in samples with hydrophobic coating can be seen on Figure 3.17 below. It has been observed through both Figure 3.16 and 3.17, that roughness is a poor predictor of hydrophobic behavior when they are coated with Cytop. However overall hydrophobic behavior (contact angles) has increased regardless of the roughness level / etch time.
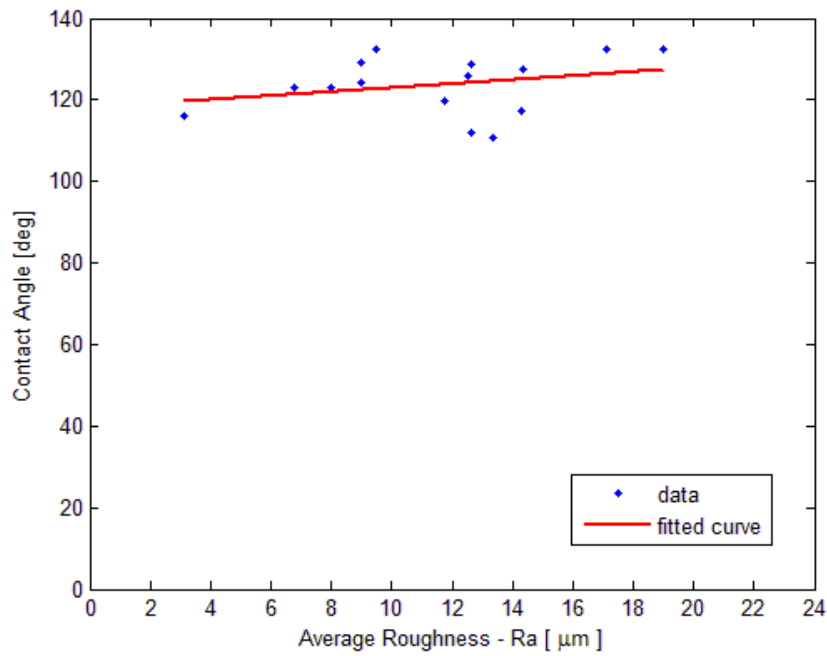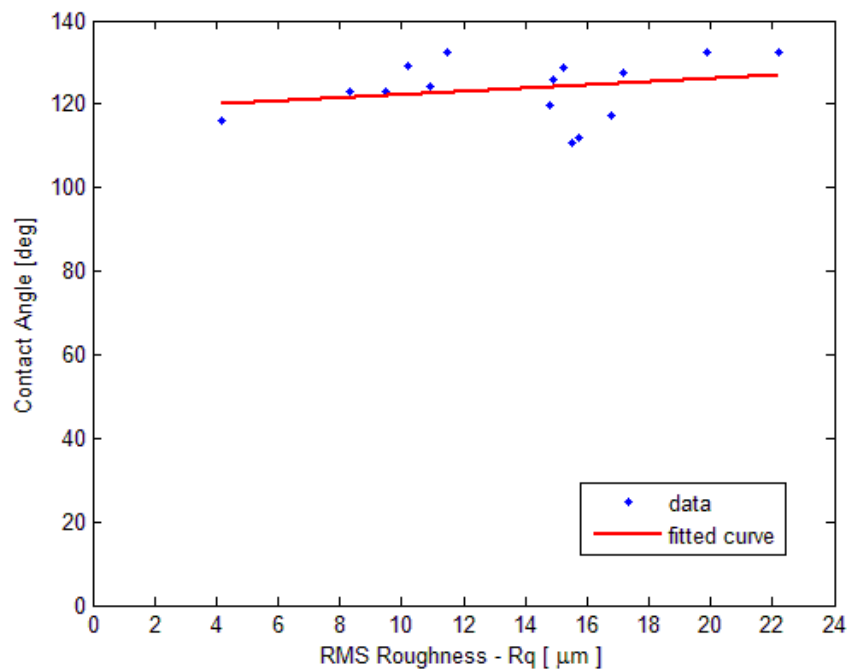
Figure 3.17: Variation of contact angle with (a) average and (b) RMS roughness respectively for hydrophobic coated samples.

For the preliminary immersion experiment to narrow down the surface type options

most suitable for corrosion resistance, six different surface types are generated which are;

40

polished, micro (etched for five minutes at 100 mA.cm^{-2}), macro texture and hydrophobic polymer (9% Cytop) coated modifications of those three groups each.

For the micro texture group, etching parameters were determined such that minimum material is removed while achieving maximum roughness. At 100 mA.cm^{-2} current density and five minutes of etching time, the optimal roughness with optimal material removal is achieved that yields desirable hydrophobic behavior when coated with Cytop.

3.3.4 Preliminary In Vitro Testing

Six groups or roughness types generated with the methods explained above are tested initially to determine the best candidates that show the best resistance to corrosion. The six roughness types tested are represented below with their corresponding names for ease of reference.

Table 3.3: Six tested roughness types on preliminary in vitro test.

Profile _____ Surface mod.	Polished	Micro (5 Min. Etch)	Macro
Uncoated	**Polished**	**Micro**	**Macro**
9% Cytop coated	**Polished C9**	**Micro C9**	**Macro C9**

Each group consists of three magnesium samples with the specified roughness type generated on their surface. Four of each group was prepared and taken out of the tank at four different time points such as 1, 2, 5 and 7 days to gather mass loss data during the 7 day period to have an idea of the mass loss rate during the test. The hydrogen collecting funnels are placed above the groups that stayed in the SBF for the longest duration which is seven days. Hydrogen gas levels are measured daily with the help of graduation lines on the tubes. In conclusion, at the end of seven days the experiment yielded the mass loss and evolved

hydrogen data. Corrosion rate data calculated using the hydrogen evolution conversion method (section 3.2.3.1) can be seen below.

The total mass loss values are calculated by subtracting the mass measurements taken after immersion from the before immersion measurements and noted on the end of each curve that represents each roughness group for ease of data reading on Figure 3.18 and Figure 3.19.
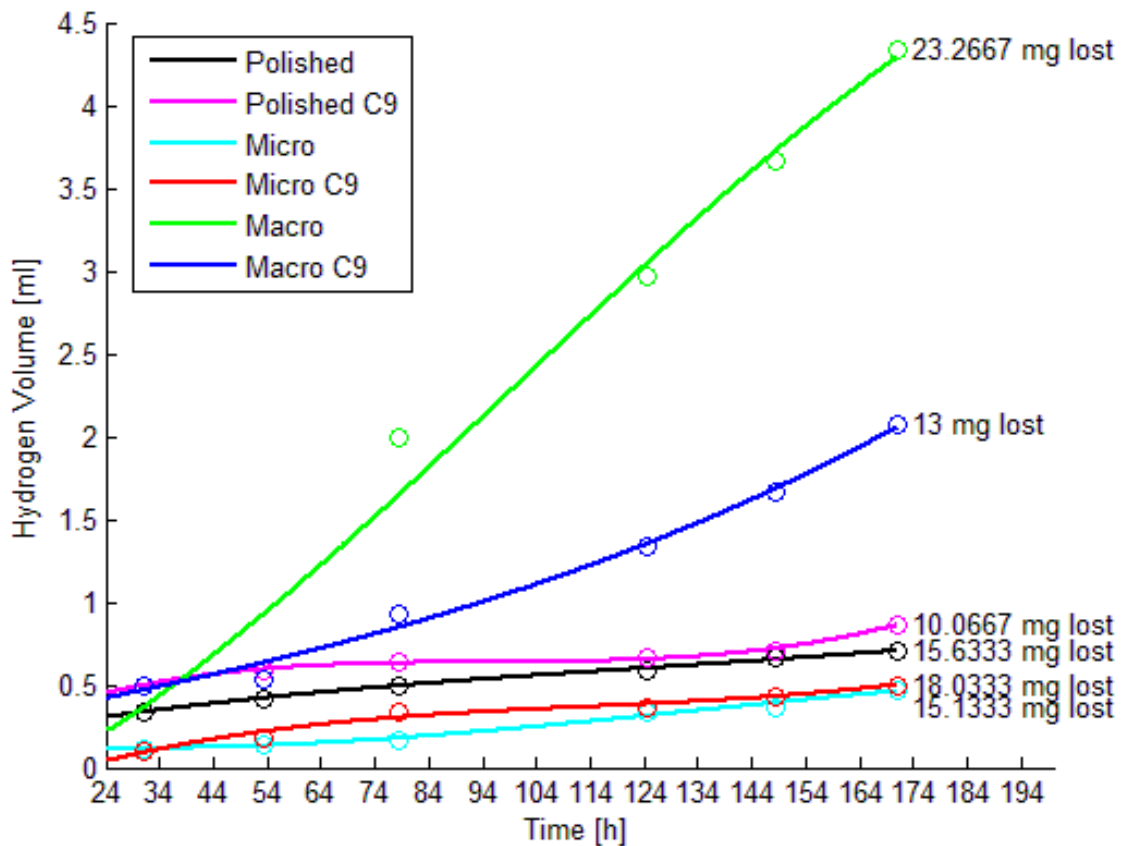
Figure 3.18: Evolved hydrogen volume over time with total mass loss at the end of seven days.
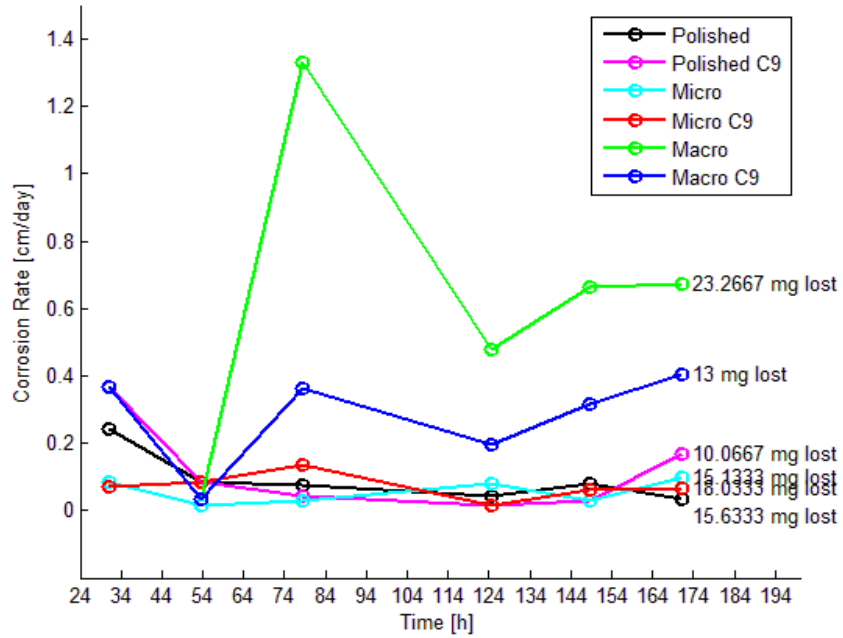
Figure 3.19: Corrosion rate over the period of seven days.
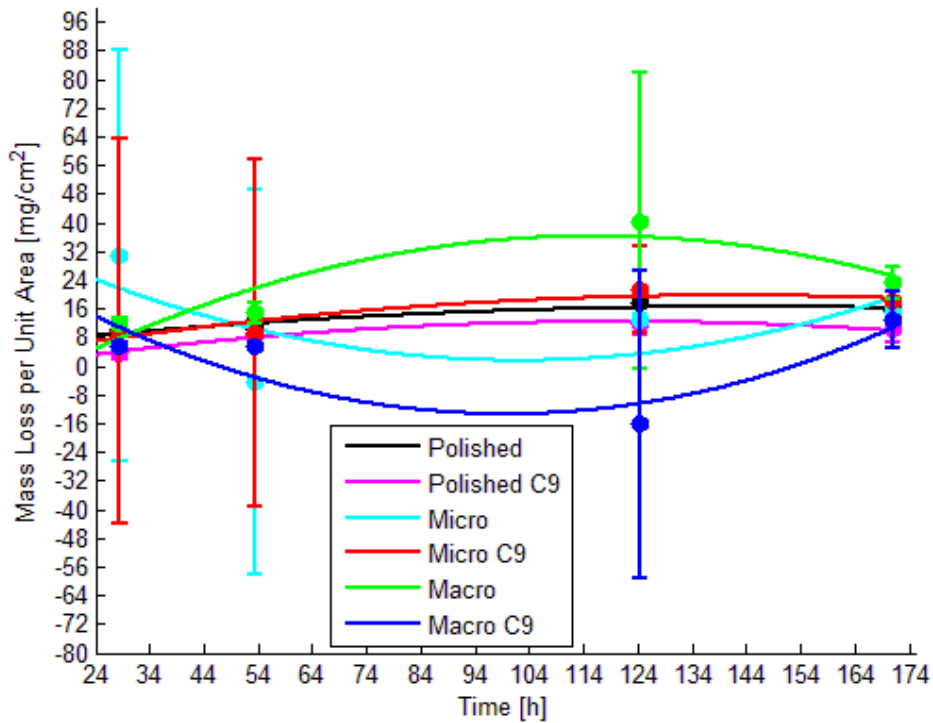
Figure 3.20: Mass loss over the period of seven days.

3.3.4.1 Discussion of Results

It has been observed that the most hydrogen was evolved from both uncoated and 9% Cytop coated macro texture groups. The coated macro group has shown slightly less gas evolution than uncoated, however the generated hydrogen in both are much higher than the polished control group. The excessive amount of hydrogen gas generation could have been caused by the increased surface area due to the extruded pillar structures on the surface. The Cytop coated macro group (which was included in the test for only experimental reasons) yielded less gas volume because the Cytop layer possibly acted as a barrier that slows down corrosion relative to the uncoated macro group.

The most promising corrosion resistance relative to the polished base group was shown by the micro groups regardless of the Cytop coating. For the follow up immersion experiment the focus is shifted on the micro groups because of that result by expanding and diversifying the process parameters to generate micro roughness samples.

The biggest problem with this initial immersion test is the inconsistency in mass measurements which can be noticed on the figures above. The mass loss in some time points goes below zero which is not expected to happen in a corrosive environment since there is no reason for the samples to gain mass during the immersion. This distortion in the mass data is most probably caused by the stop off lacquer that has been used to frame the samples to generate a consistent exposed area. During the immersion, partial peeling off of the lacquer has been observed on the samples. Furthermore, after immersion during the cleaning procedure that involves sonication in DI water, some samples completely lost their lacquer coating. Also the samples are sonicated in DI water in groups of five in average. During the sonication some lacquer was dissolved into the water and some got stuck on the

etched areas of the samples which were not possible to remove after. This irreversible transfer of lacquer between samples sonicated together is a probable explanation for the mass gain on some samples. Due to those probable reasons, the mass data is almost completely unreliable for this preliminary testing. In brief, the only reliable dataset for the preliminary testing that yields comparative results was the evolved hydrogen volume and the corrosion rate calculated by using that data (Figure 3.18 and Figure 3.19).

Another observation on Figure 3.19 is that the corrosion rates were still not converging to a low level that is desirable for biodegradable implants, which pointed for the necessity of a longer test time period for the follow up testing to observe the maximum corrosion rate period.

In summary, the preliminary testing has yielded the information that macro textures were not helping with their current texture profile to slow down corrosion, Cytop coating did not affect the corrosion resistance significantly and finally nine minute etched micro samples are promising for improved corrosion resistance. The follow up experimentation will require more diverse micro texture generating parameters, more reliable mass measurement and surface area fixation methods and finally longer experimentation time period.

3.4 Follow Up Test Samples

Following the first immersion test, the focus was shifted onto certain roughness groups and some groups were eliminated due to poor initial results in terms of corrosion resistance. The test result discussions that yielded the focus shift are documented at the end of this chapter.

On the second immersion test, polished samples are present for a second time to represent a reference as the unprocessed material texture. Micro sample diversity is increased by varying the Cytop coatings' dilution levels and adding one more hydrophobic modification using stearic acid which is going to be referred as stearic acid modification. Macro roughness group is eliminated due to poor corrosion resistance shown in preliminary in vitro testing (section 3.3.4) and kept as a future research interest.

3.4.1 Polished Surface (Base Samples)

For the follow up experimentation, the use of lacquer for exposed area consistency has been abandoned since the stop off lacquer used to fix the exposed area caused complications with the mass measurements on the preliminary testing. For the next experimentation, samples were cut into 10 x 10 mm samples cut into exact dimensions using a wire-cut EDM. The polishing procedure remained the same (see section 3.3.1) with the revised sample size and cutting procedures.
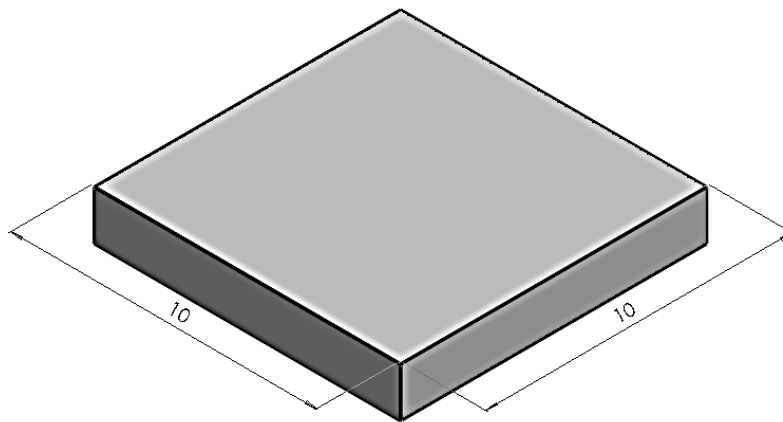
Figure 3.21: Base sample dimensions in millimeters for follow up experiment.

46

3.4.2 Micro Roughness

The etching parameters were kept the same by using the parameters determined in section 3.3.3. Samples were etched in 0.2 mol/L aqueous NaCl solution for five minutes while applying 100 mA.cm^{-2} current density. In addition to the five minute etched samples, two more groups with three and nine minutes of etching were generated one more time to observe the effect of etch duration on minimum and maximum time-points. Even though one and nine minute of etching times were the minimum and maximum durations used in section 3.3.3, three and nine minutes were picked to observe the minimum and maximum etching time effect since one minute etched samples did not yield significant roughness.

On this second step of experimentation using EDX spectroscopy, residue of chlorine (Cl) was noticed on the surface of all etched samples which was not noticed on preliminary testing preparation. Since contaminations cause magnesium alloys to show lower corrosion resistance [35], all undesired contaminations on the surface had to be removed. To remove the chlorine residue, all etched samples prepared for the follow up experiment were chemically cleaned by dipping them into a boiling solution of Chromium Trioxide and Silver Chromate for one minute. Cleaning procedure was done according to the ASTM standard [32] specified for magnesium alloys and the procedure has been applied three times to ensure complete cleansing. Samples were sonicated in DI water afterwards and dried under vacuum at 100°C for a day. The before and after cleaning EDX spectroscopy results can be seen on Figure 3.23. To ensure that the cleaning process was not etching away the base Mg alloy, a reference specimen was also dipped into the cleaning solution during the process. Near zero (≤ 0.0001 g) mass loss was observed on the reference sample after three cleaning passes.

Absence of mass loss proves that the procedure only removes the Cl contamination on the surface of the Mg alloy.

To ensure the cleaning process was not removing the desired roughness, six polished samples were etched for five minutes at 100 mA/cm^2 density and only three of them were cleaned with the ASTM boiling method. The measured average roughness for each group of three and SEM images before and after cleaning can be seen below on Figure 3.22. It has been observed that the cleaning procedure has removed the contaminations away from the pittings created with the etching, hence improving the roughness values slightly which is desirable.
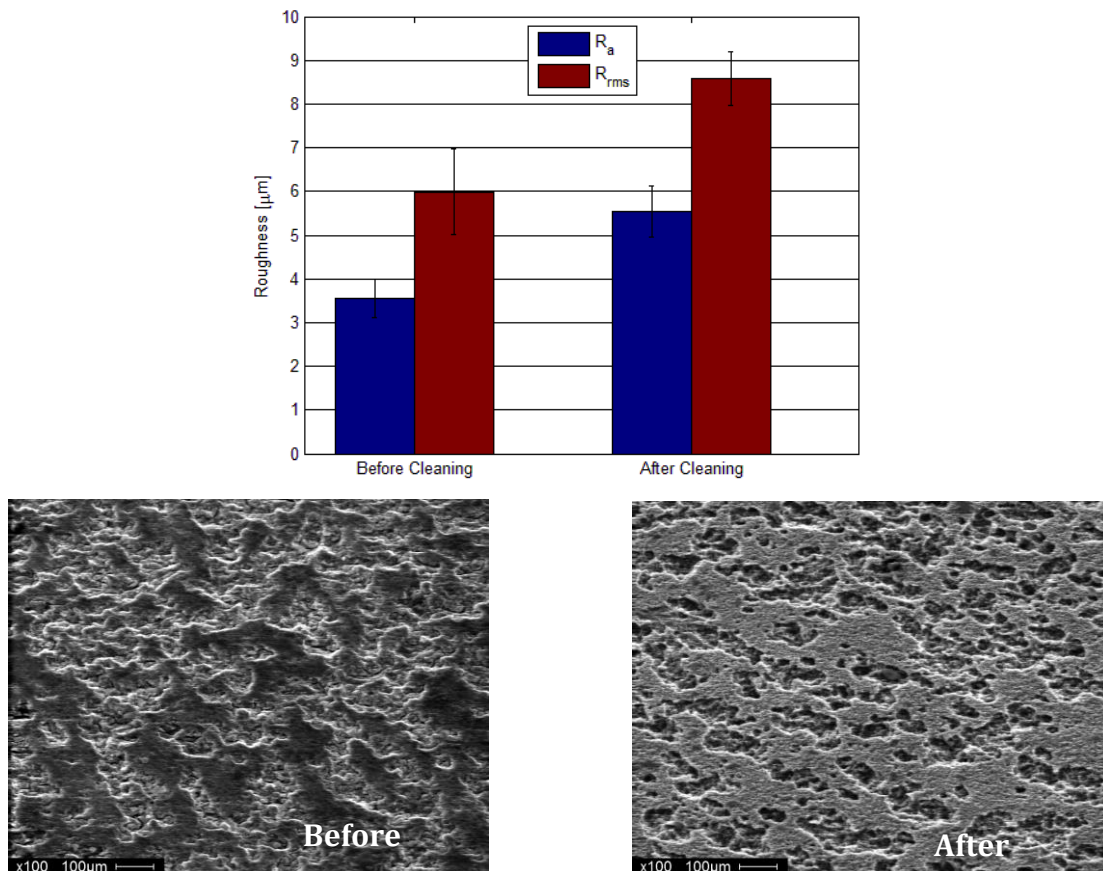
Figure 3.22: Roughness comparison after chemical cleaning procedure.
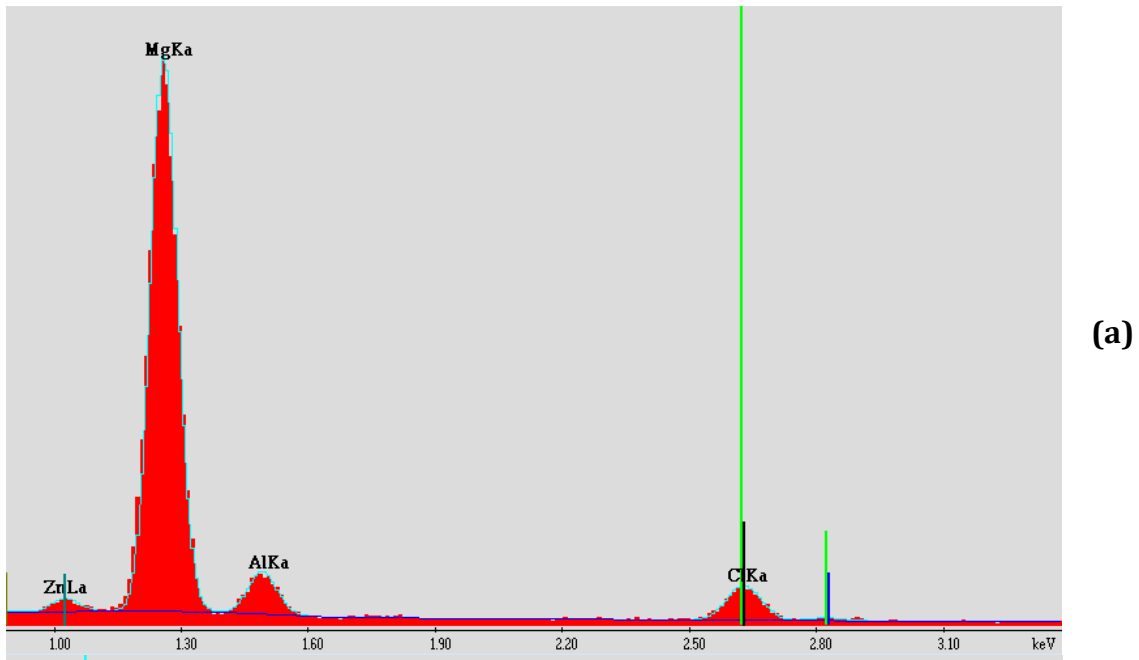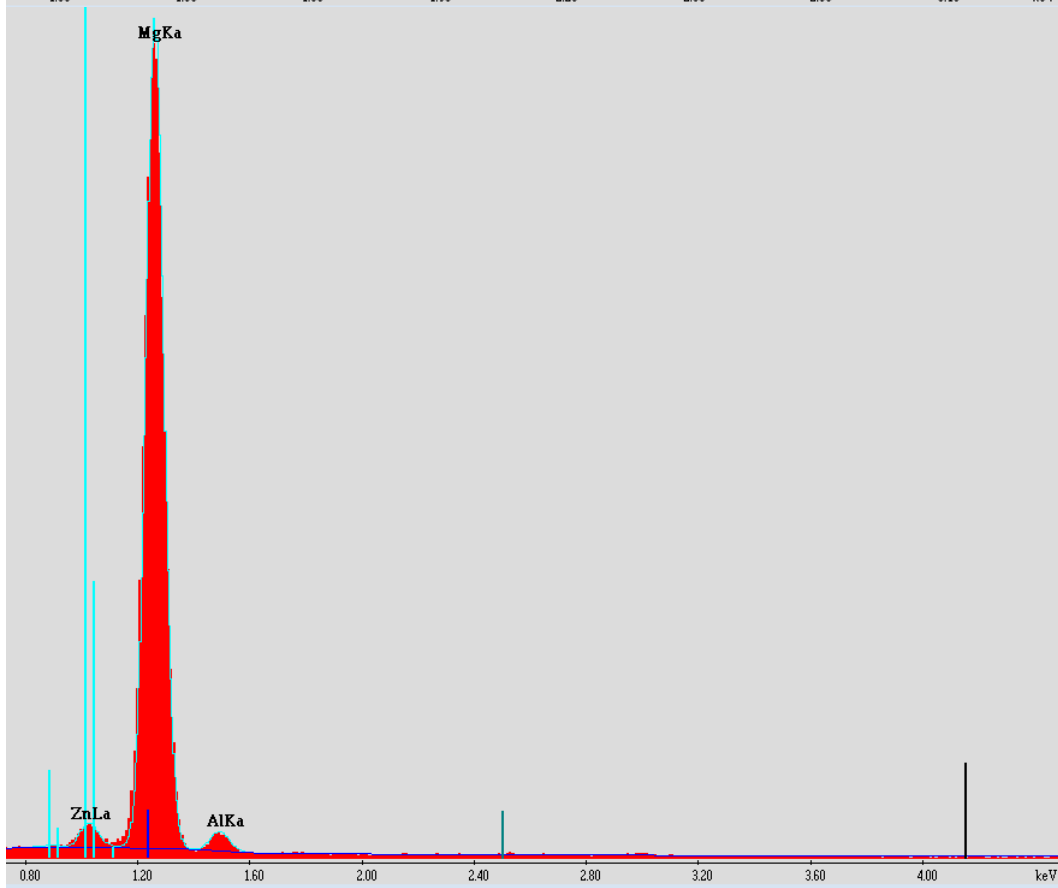
Figure 3.23: EDX Spectroscopy for etched samples (a) before chemical cleaning (b) after chemical cleaning.

49

3.4.2.1 Effect of Cytop Concentration

The effect of Cytop concentration is observed on the follow up experimentation. To achieve this, three groups of coated sample groups were created using the 9% (same concentration level used in first test), 4.5% and 2.25% concentration Cytop polymer. The coating was done using the same method explained in section 3.3.3.3.

3.4.2.2 Stearic Acid Modification

Stearic acid is a saturated fatty acid with high availability and used in cosmetics and food industry due to its bio-safety that is also one of the reasons why it was picked as a candidate for this research. It is known with its surface energy decreasing properties on metals when immersed for a certain duration [17]. Immersion of etched metal surfaces in stearic acid solution has been shown to be an alternative method of forming superhydrophobic surfaces in literature without using any polymer coating like a Cytop solution [18, 20, 36]. Parallel to Wang et al.'s paper, 0.05 mol/L ethanolic solution has been prepared using high purity ethanol and stearic acid flakes.

In order to test the effects of stearic acid on roughness profiles, one polished and three etched sample groups were prepared. Three groups of 10 x 10 mm magnesium samples are etched individually for three, five and nine minutes in 0.2 mol/L aqueous NaCl solution while applying 100 $mA.cm^{-2}$ electric current identical to the process explained in section 3.3.3. Samples are then boiled in CrO_3 and Ag_2CrO_4 solution to remove Cl contaminations off the surfaces. Subsequently, the etched and polished samples were immersed in the stearic acid solution for one hour and dried eventually.

In order to determine the hydrophobicity level of the prepared stearic acid modified samples, contact angle measurements were taken by applying the measurement method

50

explained in section 3.3.3.2. The data representation along with Cytop coatings' effect can be observed on the next section.

3.4.3 Discussion and Conclusion

One of the concerns was flattening the created roughness profile after the Cytop coating and stearic acid modifications. To ensure the roughness was not changed drastically with the modifications, profilometry measurements were taken on the nine minute etched and modified samples with different Cytop dilutions and stearic acid. Cytop layer thicknesses were also measured by coating a silicon wafer and measuring the coating thicknesses with reflectometry. Roughness and coating thickness measurements can be seen below.
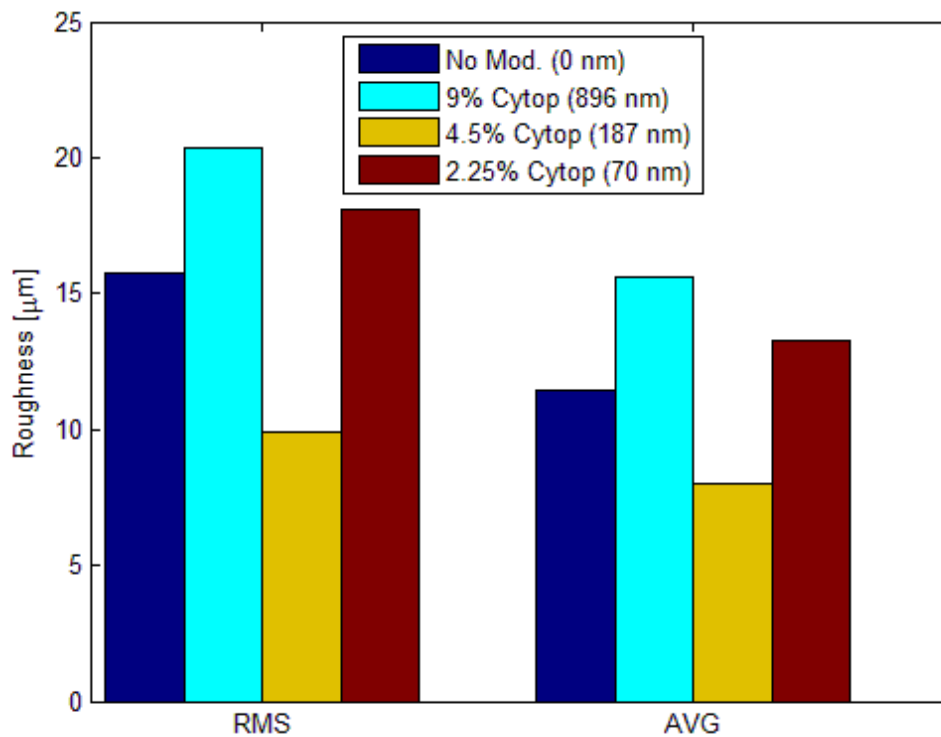
Figure 3.24: Roughness and coating thickness of each surface modification.

It has been observed that some level of smoothing occurred with 4.5% Cytop coating. The effects of this phenomenon will be accounted for when reaching to a conclusion on the discussion chapter.

New samples were prepared from batches of polished, three, five and nine minute etched samples by coating each batch individually with 9.00%, 4.50%, 2.25% Cytop solution and modifying one with stearic acid resulting in 20 different surface types for the second experiment. All samples were cleaned according to the ASTM standard before any Cytop or stearic acid modification was applied. The comparative contact angle measurements for each Cytop dilution ratio on different roughness profiles can be seen on Figure 3.25 and Figure 3.26.

(a)
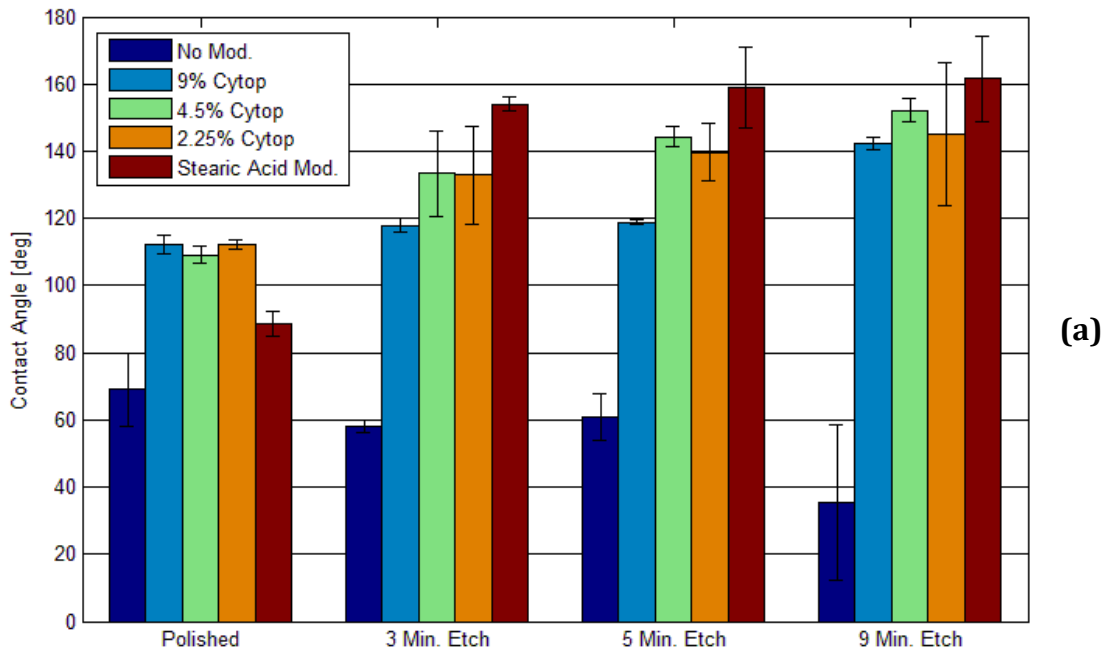
Figure 3.25: Contact angles of several surface modifications with varying roughness profiles.
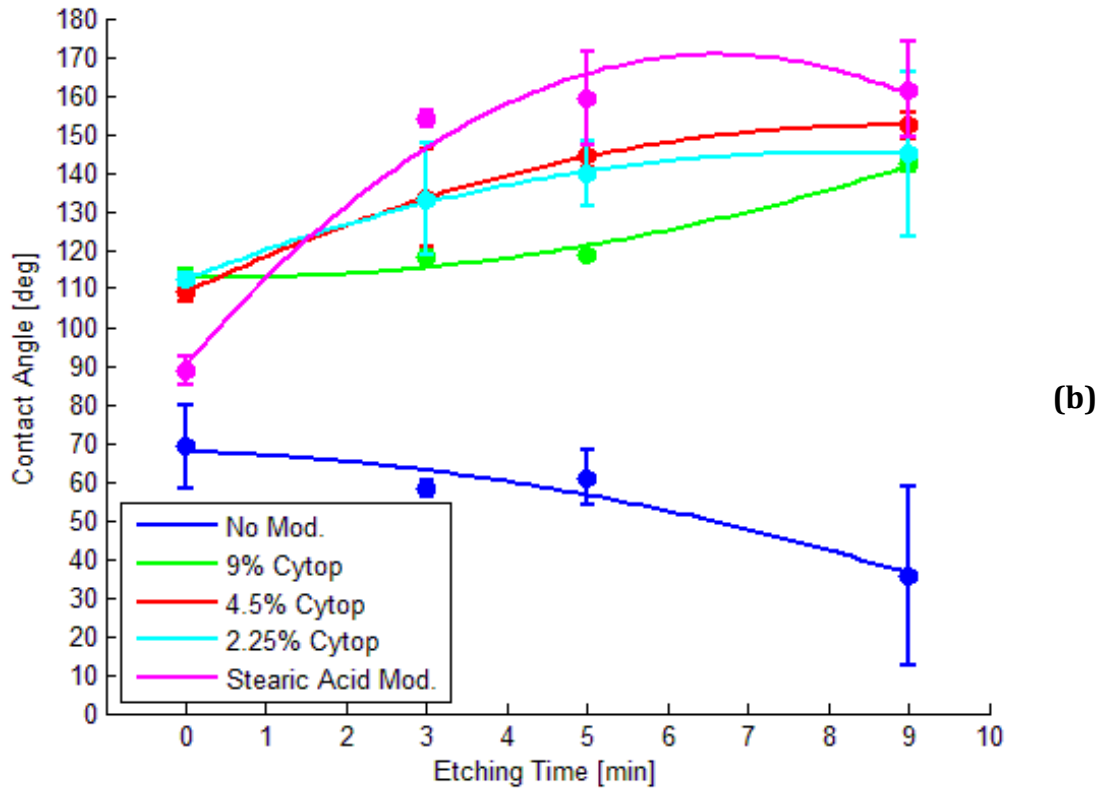
Figure 3.25 (Continued)

Compared to the reference polished smooth roughness group, without any further modifications, etching decreases the hydrophobic behavior as the etch duration increases. When the etched samples were coated in different dilutions of hydrophobic polymer (Cytop), hydrophobicity increases with increased roughness / etch duration. Finally, it has been observed that stearic acid modification yielded superhydrophobic (contact angle > 150°) properties on all etched roughness levels. Due to the nature of stearic acid modification, the hydrophobic effect is caused by a layer consisting only carbon and oxygen [20] which is desirable for biodegradability unlike Cytop coating which is a non-biodegradable polymer.

53
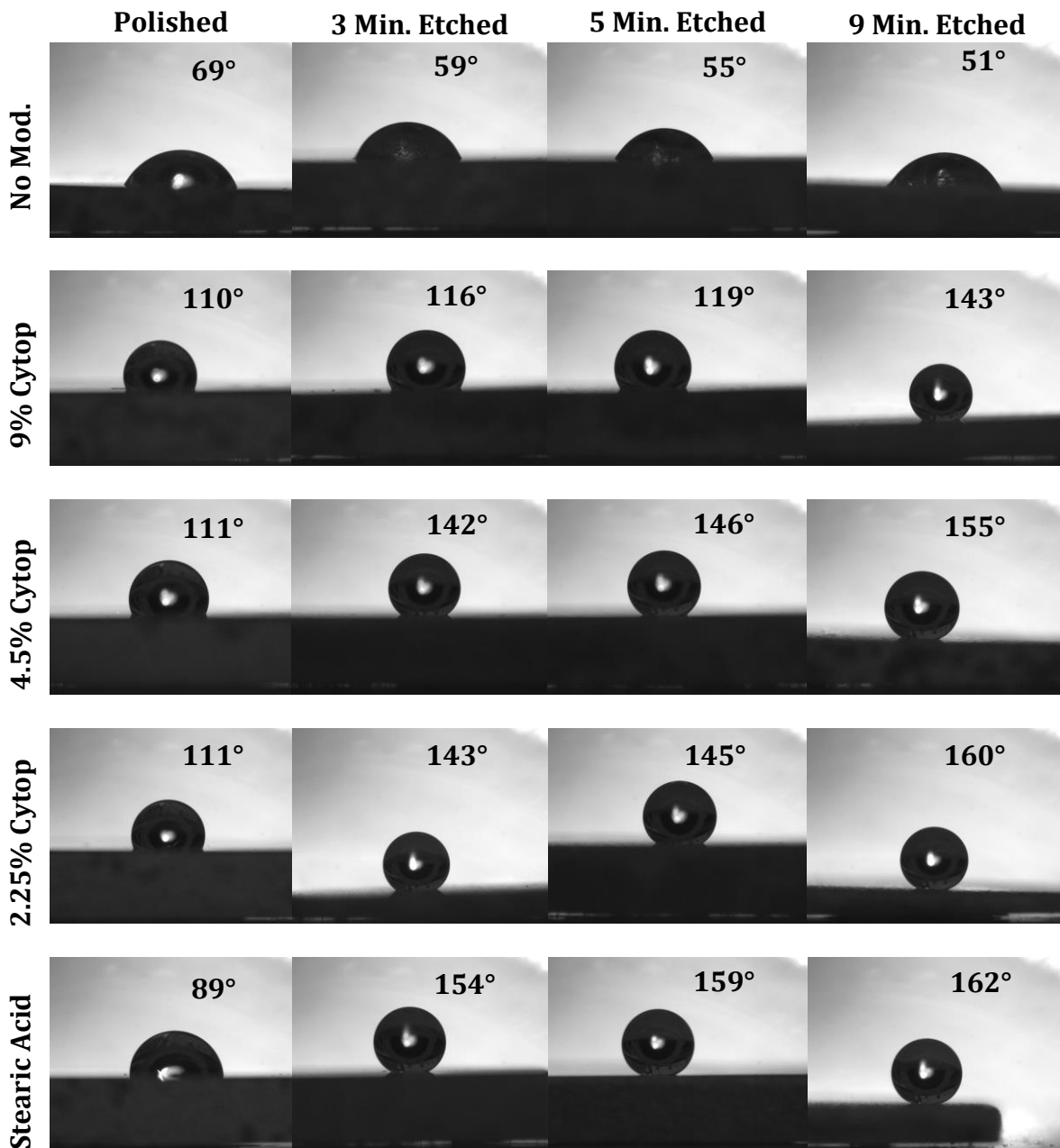
Figure 3.26: Contact angles for varying roughness profiles and surface modifications.

In conclusion, three different Cytop dilutions and stearic acid modification on different roughness profiles are tested in the simulated body environment to see their corrosion characteristics. In total, 20 different surface types are tested for this follow up experiment. Even though different dilutions of Cytop did not yield much variety in terms of

hydrophobic behavior, they are included in the experimental setup to observe the effects of these small variations. Stearic acid modification however yielded the best hydrophobicity without using any polymer coating, hence it is claimed that stearic acid group is the main focus of this follow up testing. The outcome of the experiment is discussed on Chapter 4.

CHAPTER 4: EXPERIMENTAL RESULTS

Following up the preliminary testing, the micro texture generating parameters have been diversified by adding three and nine minute etched groups along with lower dilutions of Cytop coating which are 4.5% and 2.25% in concentration. In addition to the Cytop modification, stearic acid modification's effect on corrosion speed has been observed as a biodegradable hydrophobic surface modification. The 20 roughness groups with their shortened names for ease of reference are listed below on Table 4.1

Table 4.1: 20 tested roughness types on Experiment II.

Profile Surface mod.	Polished	Micro (3 Min. Etch)	Micro (5 Min. Etch)	Micro (9 Min. Etch)
Uncoated	**Polished**	**Micro 3**	**Micro 5**	**Micro 9**
9% Cytop coated	**Polished C9**	**Micro 3-C9**	**Micro 5-C9**	**Micro 9-C9**
4.5% Cytop coated	**Polished C5**	**Micro 3-C5**	**Micro 5-C5**	**Micro 9-C5**
2.25% Cytop coated	**Polished C2**	**Micro 3-C2**	**Micro 5-C2**	**Micro 9-C2**
Stearic acid mod.	**Polished SA**	**Micro 3-SA**	**Micro 5-SA**	**Micro 9-SA**

As explained in section 3.4, the use of lacquer to fix exposed surface area has been abandoned and samples were cut into exact needed dimensions using wire EDM cutter. As a result of this, accurate mass measurements were possible since the lost / transferred lacquer mass was not an issue anymore. Also to observe the time period where maximum corrosion rate occurs, the duration of the experiment is extended from 7 to 14 days.

4.1 Mass Loss

For this test, mass measurements were not taken at different time points due to the high number of roughness groups and lack of available space within the in vitro test setup. Only before and after immersion mass measurements were taken and the resultant total

mass loss data is used as one of the measures of the corrosion resistance performance. The total mass loss data at the end of 14 days can be seen below.
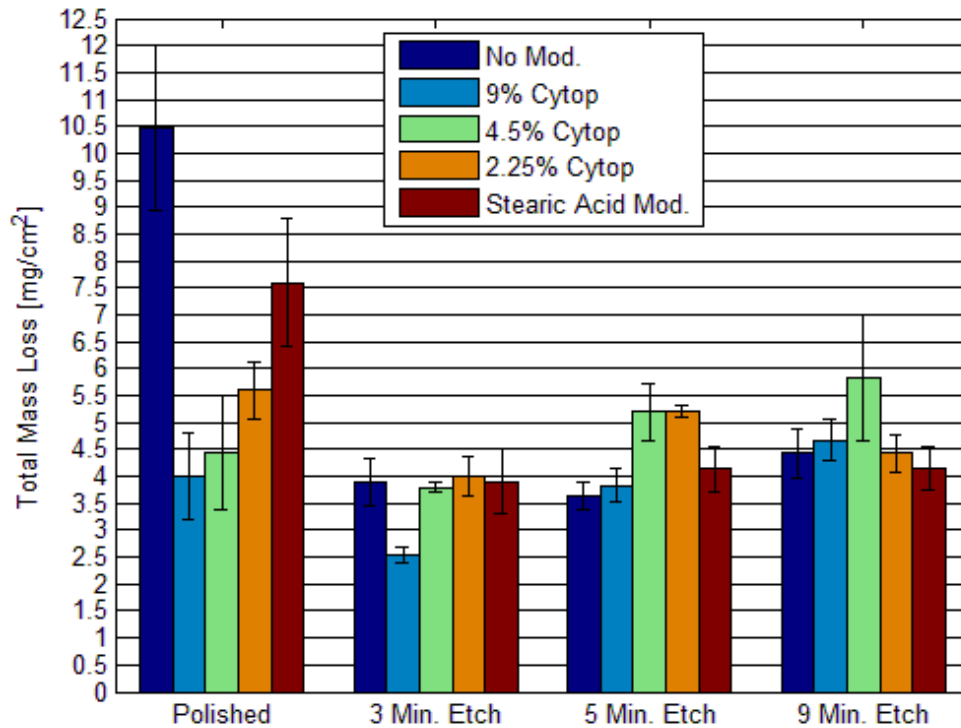
Figure 4.1: Mass loss at the end of 14 days. Error bars represent one standard deviation of the data.

To complement the corrosion rate and evolved hydrogen data, mass loss data has been plotted and 3 minute etched samples again stood out with the lowest eroded mass (Figure 4.2-a). However, contrary to expectations, samples with the lowest mass loss did not have the highest contact angle values (Figure 4.2-b).

57
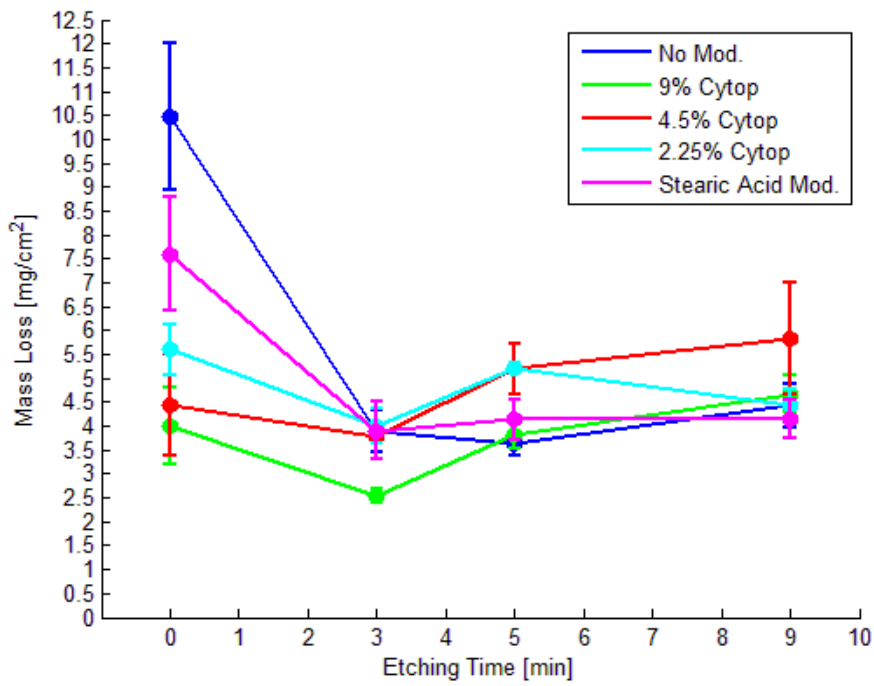
(a)
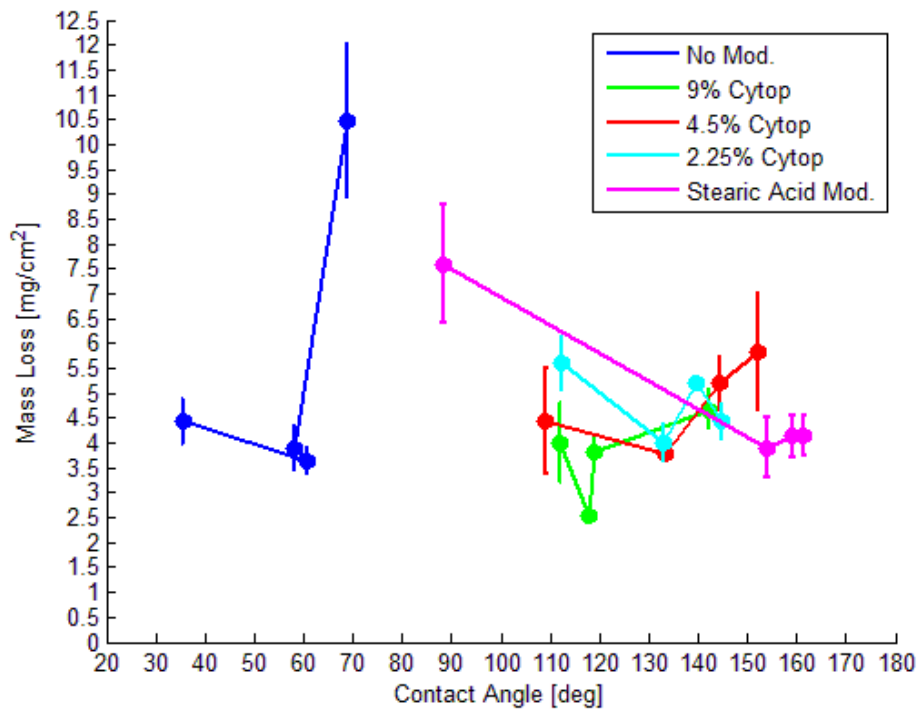
(b)

Figure 4.2: Mass loss and contact angle measurements.

58

4.2 Hydrogen Evolution

The secondary measure complementary to the mass measurements was again the hydrogen gas capturing with the method explained in section 3.2.3. Daily measurements were taken on the gas collection tubes and the volume generation rate was converted to corrosion rate using the hydrogen evolution method.

Another curiosity was whether the evolved hydrogen volume was correlated to the mass loss or not on this follow up test. The hydrogen volume vs. mass loss plot to verify the correlation is below.
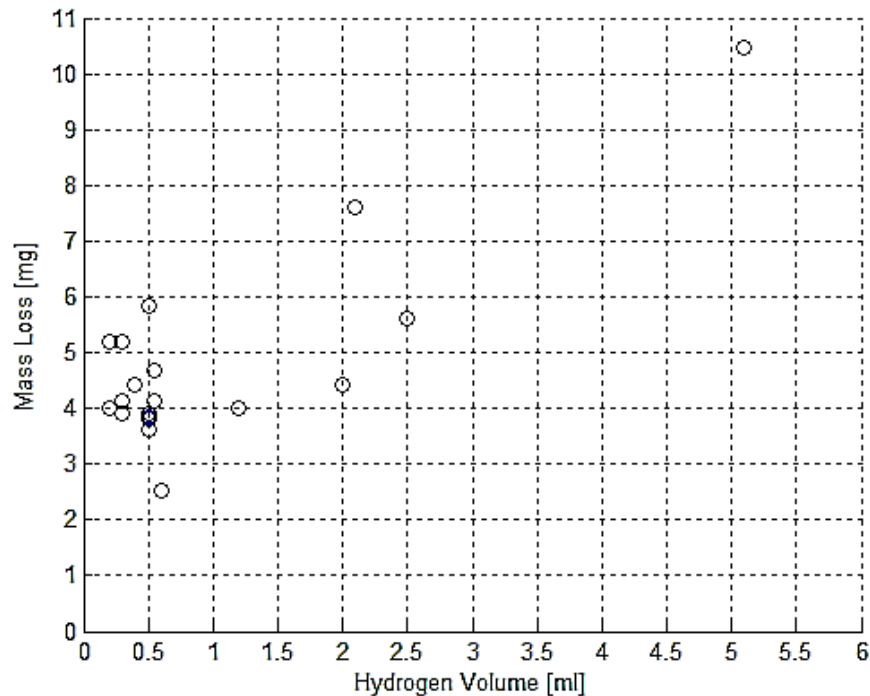
Figure 4.3: Hydrogen evolution and mass loss correlation.

The evolved hydrogen gas volume also increased with the mass loss on the samples on the long term, however within the small gas volume region, the data is distorted which is due to the lack of precision in hydrogen measurements.

59

Since there were 20 different surface types for this test, showing results on a corrosion rate vs. time plot with 20 different curves was inefficient to have an understanding of the data. Instead, the surface types were grouped under the five different surface modifications used and the data is presented with varying etching times instead of immersion duration. However, to have an idea about the time zones where the corrosion rates might have peaked, corrosion rate vs. time plots can be seen below.
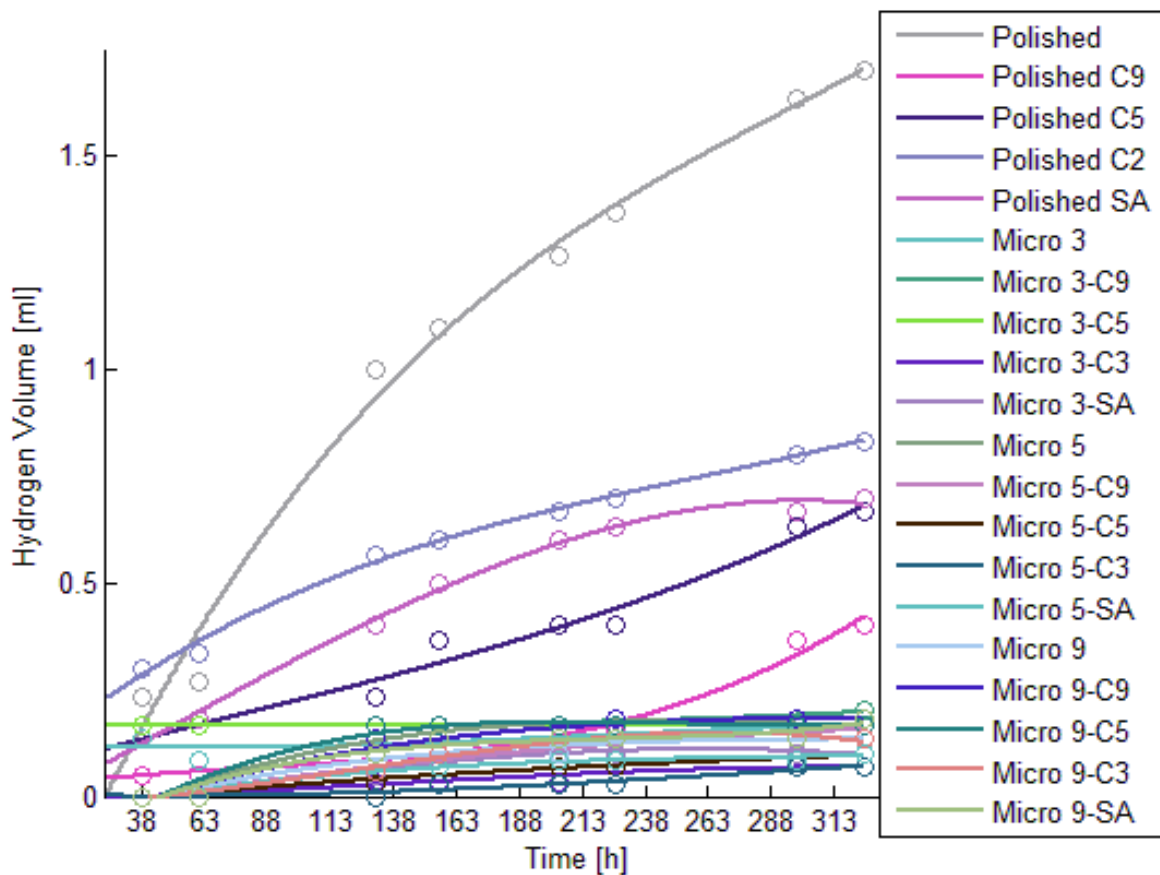
Figure 4.4: Evolved hydrogen volume.
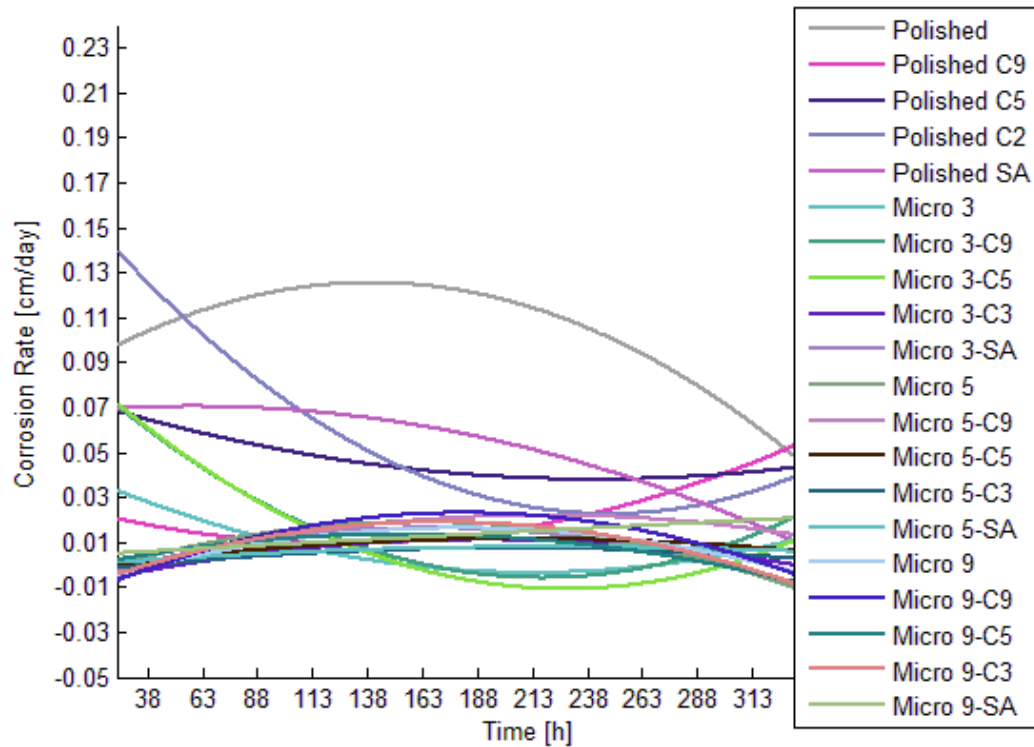
Figure 4.5: Corrosion rate

It was observed that all etched samples with or without hydrophobic modifications have shown better corrosion resistance relative to all polished groups which is a positive sign for etching and corrosion rate relation. Even though figures above were not helpful to compare the sample groups' corrosion behaviors, it was helpful to determine critical time points that corrosion rate peaked within the 14 days period. By the help of this information evolved hydrogen volume and corrosion rate were documented on the critical time points where high corrosion rates occurred. Those critical points are 131, 204 hours and 325 hours which is when the last reading taken at the end of the 14th day. The data representation can be seen on Figure 4.6 and Figure 4.7.
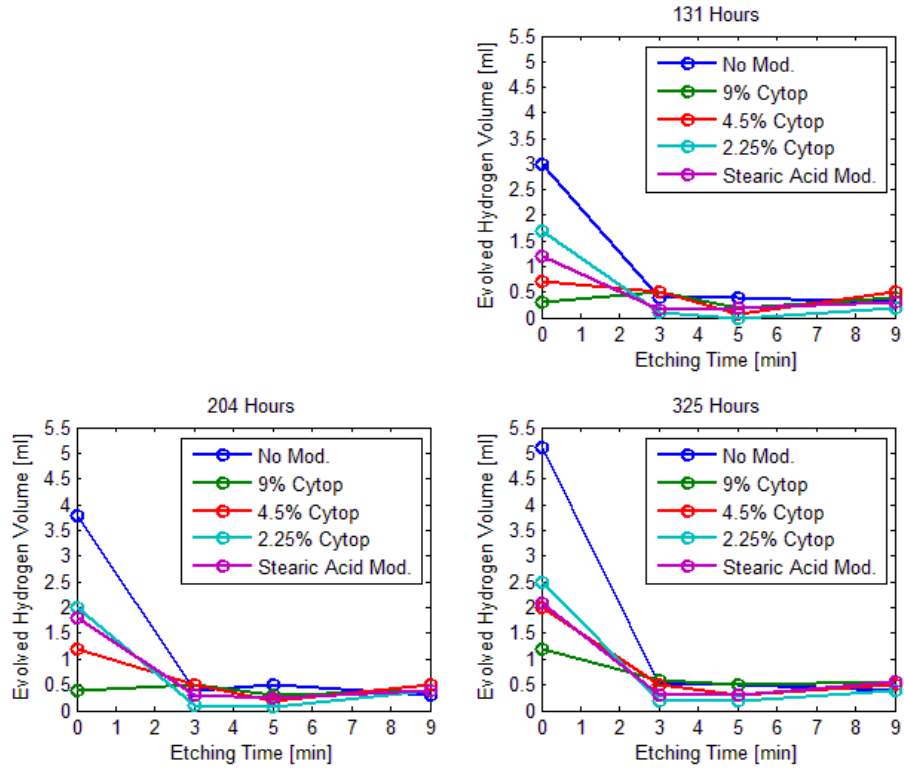
Figure 4.6: Evolved hydrogen volume on critical time points.
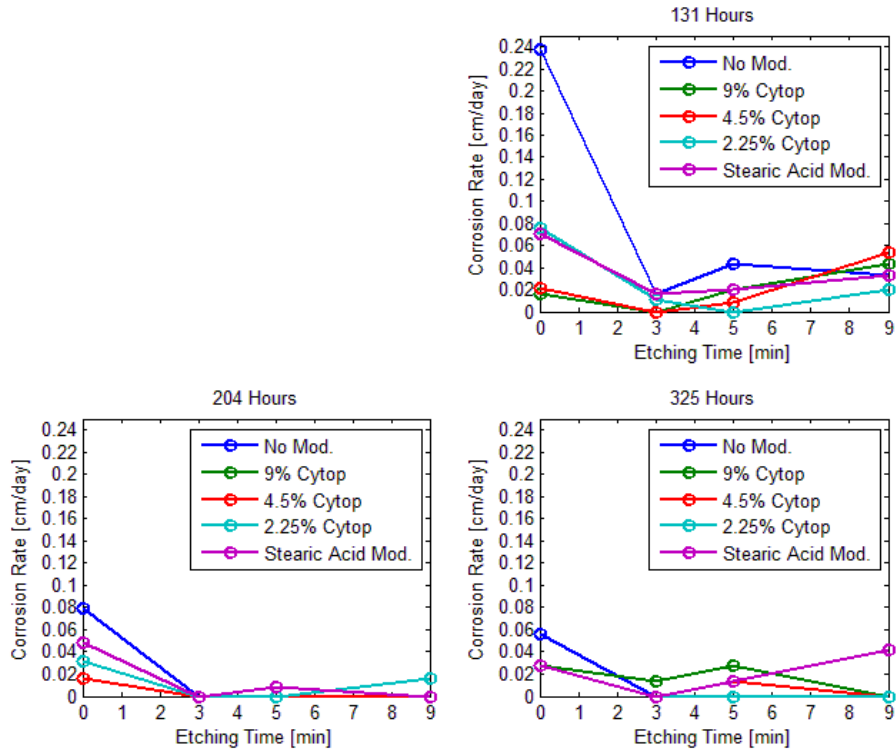
Figure 4.7: Corrosion rate on critical time points.

When the relation of evolved hydrogen volume and etching time is observed on Figure 4.6, it has been seen that all samples have yielded similar gas volumes. However, again this is due to the lack of precision in hydrogen volume measurements and smaller differences between the surface types is challenging to observe. Additionally, there is a noticeable surface group stands out from that data, which is the 3 minute etched groups that yielded the lowest corrosion rates (Figure 4.6 – 4.7) on all critical time points. When the hydrogen volume generation and corrosion rates were compared to the preliminary samples' performance on the first immersion test (Figure 3.18), similar corrosion behavior is observed for the same type of samples tested. The Cytop coated and uncoated polished samples generated approximately 0.6 mL of hydrogen at the end of 7 days during preliminary test where the same type of samples generated 0.5 to 1 mL of hydrogen at the same time point. For the five minute etched, Cytop coated and uncoated samples, the hydrogen levels were around 0.25 mL for both preliminary and follow up in vitro tests. This proved the consistency of the experimentation setup and methods.

Finally, the average of corrosion rates at all time points were taken and has been plotted to show the period of 14 days was long enough to cover the region where magnesium corrodes the fastest and causes complications in medical applications. On Figure 4.8 signs of convergence at the corrosion rate to a level that is safe for the implant receiver have been observed. However, again due to the lack of resolution on the hydrogen evolution measurements for this experiment, the conclusiveness is uncertain. Further measurements on the mass loss on different time points within the 14 day period is necessary to verify this conclusion in the future.
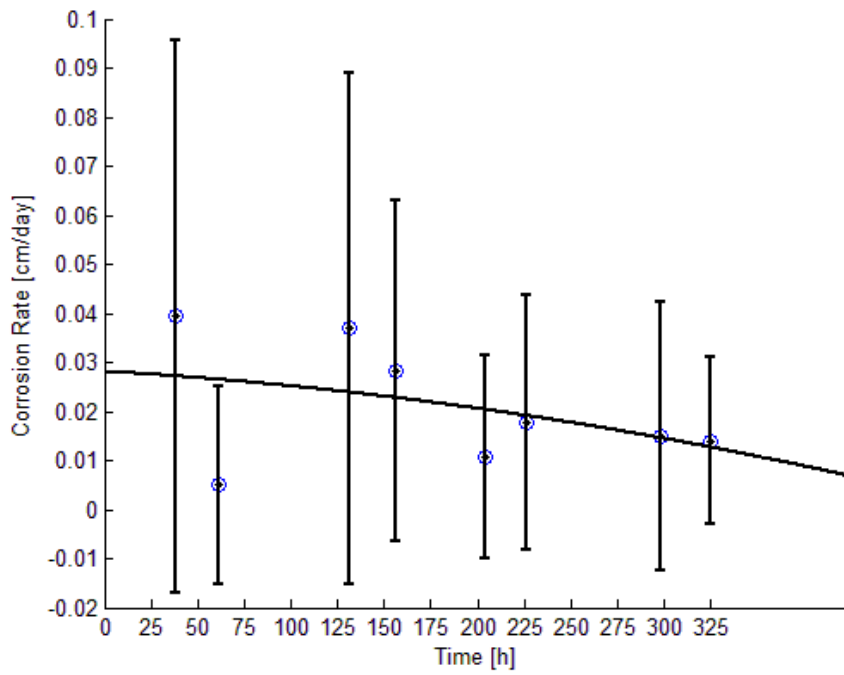
Figure 4.8: Average corrosion rate of all test groups over the course of 14 days.

CHAPTER 5: CONCLUSION

5.1 Evaluation of the Hypothesis

The hypothesis of this research was to show the possibility of changing the surface roughness such that it decreases the corrosion rate of the magnesium alloy by forming a layer of hydrogen between the magnesium alloy and the surrounding environment which is SBF in this case. The layer of gas that inhibits corrosion down to desired rates could be achieved by either generating a uniform macro structure pattern on the surface of the alloy such that generated gas bubbles due to corrosion will be trapped between the structure pattern or by giving the surface hydrophobic characteristics such that it influences evolved gas bonding onto the surface within the fluid. The use of biologically safe materials and simple methods for surface generation for consistent reproduction in the future was one of the key features of this research. Also adoption of an in vitro setup that replicates in vivo testing accurately was a unique aspects of this study that has not been tried before for corrosion characteristics of magnesium alloys with modified surfaces.

The macro pattern trials were done by creating small pillar structured patterns with the help of acid etching and stop off lacquer masking on the surfaces of AZ31 Mg alloy plates. The resultant texture did not show corrosion resistance. In contrast, due to the increased surface area the macro samples yielded the highest gas evolution and mass loss per exposed area. However due to the high variation of data due to lacquer related complications this conclusion is not trustable. The test on macro samples needed to be repeated in the future with more consistent sample preparation methods.

Micro roughness groups generated by etching the surface in aqueous NaCl solution under 100 mA.cm^{-2} current density have shown improved corrosion resistance on the preliminary in vitro testing that lasted for a week. It was observed that the etching time has influenced the roughness of the surfaces significantly between three and nine minutes. So for the follow up testing new samples were generated with three, five and nine minutes to see the effect of roughness on the corrosion speed. The samples with varying roughnesses have acted similarly (see Figure 4.1 and Figure 4.2-a). The hydrophobicity's effect was observed by coating the samples with Cytop agent or by applying stearic acid modification on the etched samples. It has been observed that increase of contact angle did not affect the corrosion resistance significantly (see Figure 4.2-b). In conclusion samples that have been etched regardless of roughness values and hydrophobic coating showed better corrosion resistance to corrosion compared to the polished control group without any significant variance with increasing roughness or hydrophobicity. The variances caused by different hydrophobic behaviors could become observable after 14 days which was not the time scope of this study. Further testing with longer durations could reveal valuable data on corrosion resistance of varying hydrophobic magnesium surfaces.

Another possible reason behind the unaffected corrosion behavior with the stearic acid modification could be the increasing dissolution rate of stearic acid in higher temperatures. All contact angle data on stearic acid modified samples were done in ambient temperature. While the solubility of stearic acid in water is 0.34 g/L at 25°C, it increases up to 1 g/L at 35°C which is nearly the operating temperature of the in vitro setup [37, 38]. Hence, there is a possibility of dissolution of the generated SA layer during the immersion test. Further studies are needed to be done to verify this phenomenon.

5.2 Comments and Future Work Recommendations

On another note, on Figure 3.12 it has been observed that, with increasing etch durations on lower current densities, the roughness also showed an increasing trend which means it might be possible to achieve greater roughness values with lower current densities or higher etch durations. This gained knowledge will be kept in consideration as an area of improvement for future research.

Another area of improvement would be on the duration of the experiments. The current time period that is 14 days gives an idea of the initial corrosion response of the samples however a test conducted for the period of at least a month would be more conclusive on the behavior. Also measuring the mass loss response at several time points similar to the method applied on the preliminary testing phase of this research would yield more confident results in terms of corrosion rate within the testing time period.

Material selection is also another point of interest. The material used in all of the experiments is the AZ31 magnesium alloy which has been a result of studies that is aimed to reduce corrosion rate by alloying, so the corrosion rate is already relatively lower. To amplify the effects of surface modifications on corrosion resistance, the use of pure magnesium would be beneficial since it has the least resistance to corrosion. The use of high reactant pure magnesium would yield data that is higher in resolution since the smallest modification would result in an observable change in corrosion behavior.

REFERENCES

1. Schinhammer, M., et al., On the Immersion Testing of Degradable Implant Materials in Simulated Body Fluid: Active pH Regulation Using CO2. Advanced Engineering Materials, 2013. 15(6): p. 434-441.

2. Kokubo, T., et al., Solutions able to reproduce in vivo surface-structure changes in bioactive glass-ceramic A-W3. Journal of Biomedical Materials Research, 1990. 24(6): p. 721-734.

3. Nutton, V., Ancient medicine. 2nd Edition ed. 2012: Routledge.

4. Park, J.B. and J.D. Bronzino, Biomaterials: principles and applications. 2002: crc press.

5. Vormann, J., Magnesium: nutrition and metabolism. Molecular aspects of medicine, 2003. 24(1): p. 27-37.

6. Hou, L.-D., et al., A review on biodegradable materials for cardiovascular stent application. Frontiers of Materials Science, 2016. 10(3): p. 238-259.

7. Witte, F., Reprint of: The history of biodegradable magnesium implants: A review. Acta Biomater, 2015. 23 Suppl: p. S28-40.

8. Degarmo, E.P.B., J.; Kohser, Ronald A., Materials and Processes in Manufacturing. 9 ed. 2003: Wiley.

9. Staiger, M.P., et al., Magnesium and its alloys as orthopedic biomaterials: a review. Biomaterials, 2006. 27(9): p. 1728-34.

10. H. Zreiqat, C.R.H., A. Zannettino, P. Evans, G. Schulze-Tanzil, C. Knabe, M. Shakibaei, Mechanisms of Magnesium-Stimulated Adhesion of Osteoblastic Cells to Commonly Used Orthopaedic Implants. Journal of biomedical materials research, 2002. 62(PART 2): p. 175-184.

11. Zeng, R.C., et al., In vitro corrosion of pure magnesium and AZ91 alloy-the influence of thin electrolyte layer thickness. Regen Biomater, 2016. 3(1): p. 49-56.

12. Zainal Abidin, N.I., et al., The in vivo and in vitro corrosion of high-purity magnesium and magnesium alloys WZ21 and AZ91. Corrosion Science, 2013. 75: p. 354-366.

68

13. Lespinasse, V.D., G. Fisher, and J.J. Eisenstaedt, A practical mechanical method of end-to-end anastomosis of blood-vessels: Using absorbable magnesium rings. Journal of the American Medical Association, 1910. 55(21): p. 1785-1790.

14. Seelig, M.G., A study of magnesium wire as an absorbable suture and ligature material. Archives of Surgery, 1924. 8(2): p. 669-680.

15. McBride, E.D., Magnesium Screw and Nail Transfixion in Fractures. Southern Medical Journal, 1938. 31.5: p. 508-514.

16. Kim, S.-M., et al., Hydroxyapatite-coated magnesium implants with improved in vitro and in vivo biocorrosion, biocompatibility, and bone response. Journal of Biomedical Materials Research Part A, 2014. 102(2): p. 429-441.

17. Wang, H., et al., A facile two-step approach to prepare superhydrophobic surfaces on copper substrates. Journal of Materials Chemistry A, 2014. 2(14): p. 5010.

18. Wang, Z., et al., Facile and fast fabrication of superhydrophobic surface on magnesium alloy. Applied Surface Science, 2013. 271: p. 182-192.

19. Liang, M., et al., Fabrication of a super-hydrophobic surface on a magnesium alloy by a simple method. Journal of Alloys and Compounds, 2016. 656: p. 311-317.

20. Wang, Y., et al., Super-hydrophobic surface on pure magnesium substrate by wet chemical method. Applied Surface Science, 2010. 256(12): p. 3837-3840.

21. Waterman, J., et al., Improvingin vitrocorrosion resistance of biomimetic calcium phosphate coatings for Mg substrates using calcium hydroxide layer. Corrosion Engineering, Science and Technology, 2013. 47(5): p. 340-345.

22. Song, G., Corrosion behavior and prevention strategies for magnesium (Mg) alloys. Corrosion Prevention of Magnesium Alloys, 2013: p. 3-65.

23. Meng, J., et al., 2—corrosion performance of magnesium (Mg) alloys containing rare-earth (RE) elements. Corrosion Prevention of Magnesium Alloys, Woodhead Publishing, 2013: p. 38-60.

24. Chen, D., et al., Biocompatibility of magnesium-zinc alloy in biodegradable orthopedic implants. Int J Mol Med, 2011. 28(3): p. 343-8.

25. Gray, J. and B. Luan, Protective coatings on magnesium and its alloys—a critical review. Journal of alloys and compounds, 2002. 336(1): p. 88-113.

26. Chen, X., M. Easton, and N. BIRBILIS, Corrosion-resistant coatings for magnesium (Mg) alloys. Corrosion Prevention of Magnesium Alloys, 2013: p. 282.

27. Dunne, C.F., et al., Corrosion behaviour of biodegradable magnesium alloys with hydroxyapatite coatings. Surface and Coatings Technology, 2016. 289: p. 37-44.

28.   Li, J., et al., Effect of heat treatment on corrosion behavior of AZ63 magnesium alloy in 3.5wt.% sodium chloride solution. Corrosion Science, 2016. 111: p. 288-301.

29.   WANG, N.-g., et al., Effect of solid solution treatment on discharge activity of AP65 magnesium alloy anode [J]. Journal of Central South University (Science and Technology), 2012. 6: p. 017.

30.   Zhao, H., K.Y. Law, and V. Sambhy, Fabrication, surface properties, and origin of superoleophobicity for a model textured surface. Langmuir, 2011. 27(10): p. 5927-35.

31.   Witte, F., et al., In vitro and in vivo corrosion measurements of magnesium alloys. Biomaterials, 2006. 27(7): p. 1013-8.

32.   ASTM, Standard Practice for Preparing, Cleaning, and Evaluation Corrosion Test Specimens, in G1-03. 2011, ASTM Standard: ASTM International, West Conshohocken, PA.

33.   Cassie, A. and S. Baxter, Wettability of porous surfaces. Transactions of the Faraday Society, 1944. 40: p. 546-551.

34.   Wang, H., et al., Fabrication of stable and corrosion-resisted super-hydrophobic film on Mg alloy. Colloids and Surfaces A: Physicochemical and Engineering Aspects, 2016. 509: p. 351-358.

35.   Supplit, R., T. Koch, and U. Schubert, Evaluation of the anti-corrosive effect of acid pickling and sol–gel coating on magnesium AZ31 alloy. Corrosion Science, 2007. 49(7): p. 3015-3023.

36.   Wang, Q., et al., Fabrication of superhydrophobic surfaces on engineering material surfaces with stearic acid. Applied Surface Science, 2008. 254(7): p. 2009-2012.

37.   Anneken, D.J., et al., Fatty Acids, in Ullmann's Encyclopedia of Industrial Chemistry. 2000, Wiley-VCH Verlag GmbH & Co. KGaA.

38.   *Properties of Substance: Stearic Acid*. 2007   [cited 2016 10/21]; Available from: http://chemister.ru/Database/properties-en.php?dbid=1&id=4852.

APPENDIX A: VALIDATION OF HYDROGEN EVOLUTION WITH STOICHIOMETRIC

APPROACH

$$Exposed\ surface\ area\ of\ Mg = A = 1\ cm^2$$

$$Inputs = \begin{bmatrix} 0 & \text{Hydrogen Evolved (mL)} & \text{Time (h)} \\ 31\ h & 0.35 & 31 \\ 53.5\ h & 0.05 & 22.5 \\ 78.5\ h & 0.10 & 25 \\ 124.5\ h & 0.50 & 46 \\ 148.5\ h & 0.10 & 24 \\ 171\ h & 0.30 & 22.5 \end{bmatrix}$$

$$V_{hydrogen} = \begin{bmatrix} 0.35 \\ 0.05 \\ 0.10 \\ 0.50 \\ 0.10 \\ 0.30 \end{bmatrix} . mL \qquad time = \begin{bmatrix} 31 \\ 22.5 \\ 25 \\ 46 \\ 24 \\ 22.5 \end{bmatrix} . h . \frac{day}{24h}$$

Following calculations are done based on those evolved hydrogen volume ($V_{hydrogen}$)

and time input matrices.

$$\dot{V} = \frac{V_{hydrogen}}{time} \qquad \rho_{hydrogen} = 0.00008375\ \frac{g}{mL}$$

$$\dot{m}_{hydrogen} = \dot{V} . \rho_{hydrogen}$$

$$\dot{m}_{hydrogen} = \begin{bmatrix} 3.94\ x\ 10^{-8} \\ 7.75\ x\ 10^{-9} \\ 1.40\ x\ 10^{-8} \\ 3.79\ x\ 10^{-8} \\ 1.45\ x\ 10^{-8} \\ 4.65\ x\ 10^{-8} \end{bmatrix} . \frac{g}{day}$$

Convert grams to moles by dividing the mass loss rate by molar mass of hydrogen

which is 2 grams/mol.

$$\dot{mol}_{hydrogen} = \frac{\dot{m}_{hydrogen}}{2} \cdot \frac{mol}{g} = \begin{bmatrix} 1.97\ x\ 10^{-8} \\ 3.88\ x\ 10^{-9} \\ 6.98\ x\ 10^{-9} \\ 1.90\ x\ 10^{-8} \\ 7.27\ x\ 10^{-9} \\ 2.33\ x\ 10^{-8} \end{bmatrix} \cdot \frac{mol}{day}$$

Corrosion of one mole of magnesium yields one mole of hydrogen gas. To calculate mass of magnesium, mole value is multiplied by molar mass of magnesium which is 24 grams/mole.

$$\dot{m}_{magnesium} = \dot{mol}_{hydrogen} \cdot 24 \frac{g}{mol} = \begin{bmatrix} 4.73\ x\ 10^{-7} \\ 9.31\ x\ 10^{-8} \\ 1.68\ x\ 10^{-7} \\ 4.55\ x\ 10^{-7} \\ 1.74\ x\ 10^{-7} \\ 5.58\ x\ 10^{-7} \end{bmatrix} \cdot \frac{g}{day}$$

$$MassLoss = \frac{\dot{m}_{magnesium}}{A} = \begin{bmatrix} 4.73\ x\ 10^{-7} \\ 9.31\ x\ 10^{-8} \\ 1.68\ x\ 10^{-7} \\ 4.55\ x\ 10^{-7} \\ 1.74\ x\ 10^{-7} \\ 5.58\ x\ 10^{-7} \end{bmatrix} \cdot \frac{g}{cm^2 . day}$$

$$CR_{stoichiometry} = \frac{MassLoss}{\rho_{magnesium}} = \begin{bmatrix} 2.58\ x\ 10^{-7} \\ 5.07\ x\ 10^{-8} \\ 9.13\ x\ 10^{-8} \\ 2.48\ x\ 10^{-7} \\ 9.51\ x\ 10^{-8} \\ 3.04\ x\ 10^{-7} \end{bmatrix} \cdot \frac{cm}{day} \qquad Timepoints = \begin{bmatrix} 31 \\ 53.5 \\ 78.5 \\ 124.5 \\ 148.5 \\ 171 \end{bmatrix} \cdot hour$$

$$CR_{lespinasse} = \begin{bmatrix} 2.56\ x\ 10^{-7} \\ 5.05\ x\ 10^{-8} \\ 9.13\ x\ 10^{-8} \\ 2.47\ x\ 10^{-7} \\ 9.51\ x\ 10^{-8} \\ 3.02\ x\ 10^{-7} \end{bmatrix} \cdot \frac{cm}{day} \qquad Error = \frac{CR_{lespinasse} - CR_{stoichiometry}}{CR_{stoichiometry}} x100 \approx 0$$

APPENDIX B: G-CODE FOR CNC MACRO TEXTURE GENERATION

MatLab code used to generate the g-code is below.

```
%% inputs
borderlength_o = 13; %outer border
dimension
borderlength_i = 11; %inner border
dimension
borderdensity = 0.5; %border dot spacing
%% parameters
syms x y G
step = 1/borderdensity;
blength_o = borderlength_o*step;
blength_i = borderlength_i*step;
blength = blength_o;
%% first dot
G = [ 'G91           ';
     'F100          '];
G = [G;'G1 X0.0  Y0.0  Z1.0 '];
G = [G;'G1 X1.0  Y1.0  Z0.0 '];
G = [G;'G1 X0.0  Y0.0  Z-1.0 '];
G = [G;'G1 X0.0  Y0.0  Z1.0 '];
%% Border
for blength=blength_o:-step:blength_i
for n=1:1:blength
  G = [G;'G1 X0.5  Y0.0  Z0.0 '];
  G = [G;'G1 X0.0  Y0.0  Z-1.0 '];
  G = [G;'G1 X0.0  Y0.0  Z1.0 '];
end
for n=1:1:blength
  G = [G;'G1 X0.0  Y0.5  Z0.0 '];
  G = [G;'G1 X0.0  Y0.0  Z-1.0 '];
  G = [G;'G1 X0.0  Y0.0  Z1.0 '];
end
for n=1:1:blength
  G = [G;'G1 X-0.5 Y0.0  Z0.0 '];
  G = [G;'G1 X0.0  Y0.0  Z-1.0 '];
  G = [G;'G1 X0.0  Y0.0  Z1.0 '];
end
for n=1:1:blength
  G = [G;'G1 X0.0  Y-0.5 Z0.0 '];
  G = [G;'G1 X0.0  Y0.0  Z-1.0 '];
  G = [G;'G1 X0.0  Y0.0  Z1.0 '];
end
if blength>blength_i
  G = [G;'G1 X0.5  Y0.5  Z0.0 '];
  G = [G;'G1 X0.0  Y0.0  Z-1.0 '];
  G = [G;'G1 X0.0  Y0.0  Z1.0 '];
end
end
%% Dots
  G = [G;'G1 X0.5  Y0.5  Z0.0 ']; %first dot
  G = [G;'G1 X0.0  Y0.0  Z-1.0 '];
  G = [G;'G1 X0.0  Y0.0  Z1.0 '];
for t=1:1:5
for k=1:1:10
  G = [G;'G1 X1.0  Y0.0  Z0.0 '];
  G = [G;'G1 X0.0  Y0.0  Z-1.0 '];
  G = [G;'G1 X0.0  Y0.0  Z1.0 '];
  if k==10
  G = [G;'G1 X0.5  Y1.0  Z0.0 '];
  G = [G;'G1 X0.0  Y0.0  Z-1.0 '];
  G = [G;'G1 X0.0  Y0.0  Z1.0 '];
  end
end
for k=1:1:11
  G = [G;'G1 X-1.0 Y0.0  Z0.0 '];
  G = [G;'G1 X0.0  Y0.0  Z-1.0 '];
  G = [G;'G1 X0.0  Y0.0  Z1.0 '];
  if k==11
  G = [G;'G1 X0.5  Y1.0  Z0.0 '];
  G = [G;'G1 X0.0  Y0.0  Z-1.0 '];
  G = [G;'G1 X0.0  Y0.0  Z1.0 '];
  end
end
  if t==5
  for k=1:1:10
  G = [G;'G1 X1.0  Y0.0  Z0.0 '];
  G = [G;'G1 X0.0  Y0.0  Z-1.0 '];
  G = [G;'G1 X0.0  Y0.0  Z1.0 '];
  end
  end
end
%% Display
disp(G)
fid = fopen('gcode.gcode','wt');
for ii = 1:size(G,1)
  fprintf(fid,'%s\t',G(ii,:));
  fprintf(fid,'\n');
end
fclose(fid)
```

73

APPENDIX C: MICROCONTROLLER CODE FOR SIMULATED BODY ENVIRONMENT

AUTOMATION

```
#include "max6675.h"          //max6675 temperature sensor
#include <UTFT.h>             //16bit TFT screen library
#include <SD.h>            //SD card library
#include <SPI.h>            //SD related
#include <Wire.h>             //One Wire library
#include "RTClib.h"           //Real Time Clock library
#include <EEPROMex.h>          //Extended Eeprom library

RTC_DS1307 rtc;              //Define RTC module

// PIN CONNECTIONS //
const int chipSelect = 49;       //pin for chipselect SD card
int ktcSO = 5;            //max6675
int ktcCS = 6;            //max6675
int ktcCLK = 7;           //max6675
int co2valve = 3;           //CO2 solenoid pin (relay)
int heaterPin = 46;          //pin for Heater (relay)
int heaterPinGround = 47;       //ground for Heater

// VARIABLES //
float tempRead;
String inputstring = "";                //a string to hold incoming data from the PC
String sensorstring = "";                //a string to hold the data from the Atlas Scientific product
boolean input_string_complete = false;        //have we received all the data from the PC
boolean sensor_string_complete = false;        //have we received all the data from the Atlas Scientific
product
float pH;                   //used to hold a floating point number that is the pH
float pHcorrected;
float Temp = 36.5;               // Set temperature
float TempK = Temp + 273.15;            // Convert to Kelvin
float setpH = 7.40;            // set pH
float setpHbuffer = 0.15;           // set pH tolerance
float DigitalTemp = Temp;             // This is the initial value that will be replaced by the calc
later

extern uint8_t BigFont[];          // Which fonts to use...
extern uint8_t SevenSegNumFont[];
extern uint8_t SmallFont[];

int sdState = LOW;         //variables for delayed writing to SD card
long sdPreviousMillis = 0;           //       |
long sdTime = 2000;            //       |

MAX6675 ktc(ktcCLK, ktcCS, ktcSO);
```

74

```
UTFT myGLCD(SSD1289, 38, 39, 40, 41);      //pins and chip used for TFT
DateTime now;                        //call current Date and Time

void setup()
{
 // initialize the digital pins as an output:
 pinMode(heaterPin, OUTPUT);
 pinMode(heaterPinGround, OUTPUT);
 digitalWrite(heaterPinGround, LOW);
 pinMode(co2valve, OUTPUT);
 pinMode(chipSelect, OUTPUT);              //SD card
 digitalWrite(chipSelect, HIGH);
 pinMode(SS, OUTPUT);
 Serial.begin(9600);
 Serial3.begin(9600);  //set baud rate for software serial port_3 to 9600
 delay(500);       // give the MAX6675 a little time to settle
 SDSetup();
 LCDsetup();
 timeSetup();
}

void loop()
{
// timeLoop();
 tempLoop();
 phLoop();
 SDLoop();
 LCDloop();
}

void serialEvent()
{
 inputstring = Serial.readStringUntil(13); //read the string until we see a <CR>
 input_string_complete = true;              //set the flag used to tell if we have received a completed
string from the PC
}

void serialEvent3()
{
 sensorstring = Serial3.readStringUntil(13);       //read the string until we see a <CR>
 sensor_string_complete = true;              //set the flag used to tell if we have received a completed
string from the PC
}

void timeSetup()
{
 Wire.begin();
 rtc.begin();
 //rtc.adjust(DateTime(F(__DATE__), F(__TIME__))); //uncomment this once and upload. Then
comment it out and upload again
 //This will set the time the first time you upload it and if you don't upload again with it commented
out it will
 //reset the clock to the time the code was compliled each time.
}
```

75

```
void SDLoop()
{
 unsigned long sdCurrentMillis = millis();
 if (sdCurrentMillis - sdPreviousMillis > sdTime)
 {
  sdPreviousMillis = sdCurrentMillis;
  if (sdState == LOW)
  {
   sdState = HIGH;
   File dataFile = SD.open("datalog.csv", FILE_WRITE);

   if (dataFile)
   {
    now = rtc.now();
    dataFile.print(now.month(), DEC);
    dataFile.print('/');
    dataFile.print(now.day(), DEC);
    dataFile.print('/');
    dataFile.print(now.year(), DEC);
    dataFile.print(", ");
    dataFile.print(now.hour(), DEC);
    dataFile.print(':');
    dataFile.print(now.minute(), DEC);
    dataFile.print(':');
    dataFile.print(now.second(), DEC);
    dataFile.print(", ");
    dataFile.print((float)(pH), 2);
    dataFile.print(", ");
    dataFile.print((float)(tempRead), 2);

    dataFile.println();
    dataFile.close();

    myGLCD.setFont(SmallFont);
    myGLCD.setColor(0, 255, 0);
    myGLCD.print("Last log entry on", 5, 225);
    myGLCD.printNumI(now.hour(), 153, 225);
    myGLCD.print(":", 166, 225);
    myGLCD.printNumI(now.minute(), 170, 225);
    myGLCD.print(":", 183, 225);
    myGLCD.printNumI(now.second(), 187, 225);

   }
  }
  else
  {
   sdState = LOW;
   myGLCD.setFont(SmallFont);
  }
 }
}

void tempLoop()
{
 tempRead = ktc.readCelsius();
```

76

```
   if (tempRead < DigitalTemp)
   {
     digitalWrite(heaterPin, HIGH);
     myGLCD.setColor(255, 0, 0);
     myGLCD.fillCircle(38, 124, 5);
     delay(200);
   }

   else if ( tempRead >= DigitalTemp)
   {
     digitalWrite(heaterPin, LOW);
     myGLCD.setColor(192, 192, 192);
     myGLCD.fillCircle(38, 144, 5);
     delay(200);

   }
}

void phLoop()
{
  if (input_string_complete == true)              //if a string from the PC has been received in its entirety
  {
    Serial3.print(inputstring);                 //send that string to the Atlas Scientific product
    Serial3.print('\r');                 //add a <CR> to the end of the string
    inputstring = "";                 //clear the string
    input_string_complete = false;              //reset the flag used to tell if we have received a completed
string from the PC
  }


  if (sensor_string_complete == true)              //if a string from the Atlas Scientific product has been
received in its entirety
  {
    Serial.println(sensorstring);              //send that string to the PC's serial monitor
    if (isdigit(sensorstring[0]))              //if the first character in the string is a digit
    {
      pH = sensorstring.toFloat();                //convert the string to a floating point number so it can be
evaluated by the Arduino
      pHcorrected = 7.0 + (pH - 7.0) * ((tempRead + 273.15) / 298.15); // pH conversion factoring in the
temperature
    }
  }
  sensorstring = "";                          //clear the string:
  sensor_string_complete = false;              //reset the flag used to tell if we have received a completed
string from the Atlas Scientific product

  if (pHcorrected > setpH + setpHbuffer)
  {
    digitalWrite(co2valve, LOW);
    myGLCD.setColor(255, 0, 0);
    myGLCD.fillCircle(38, 144, 5);
    delay(500);
  }
  else
  {
```

77

```
     digitalWrite(co2valve, HIGH);
     myGLCD.setColor(192, 192, 192);
     myGLCD.fillCircle(38, 144, 5);

 }
 }

 void SDSetup()
 {
  if (!SD.begin(chipSelect))
  {
   return;
  }
 }

 void LCDsetup()
 {
  myGLCD.InitLCD(LANDSCAPE);     //LANDSCAPE or PORTRAIT
  myGLCD.clrScr();
  mainscr();               //Default screen is mainscr
 }
 void LCDloop()
 {
  myGLCD.setFont(BigFont);
  myGLCD.setColor(255, 255, 255);
  // myGLCD.printNumF(pH, 2, 140, 70); //location value pH
  myGLCD.printNumF(tempRead, 1, 140, 116); //location value Temp
  myGLCD.printNumF(pHcorrected, 2, 140, 136); //temperature influenced pH

 }
 void mainscr()
 {
  myGLCD.fillScr(0, 87, 60);
  myGLCD.setBackColor(0, 87, 60);
  myGLCD.setFont(BigFont);
  myGLCD.setColor(255, 255, 255);

  // myGLCD.print("  pH", 60, 70);
  myGLCD.print("Temp", 60, 116);
  myGLCD.print("C", 215, 116); //degree celcius
  myGLCD.print("  pH", 60, 136);


  myGLCD.setFont(BigFont);
  myGLCD.setColor(255, 255, 255);
  myGLCD.print("UNIVERSITY OF SOUTH", 5, 10);
  myGLCD.print("     FLORIDA", 5, 30);

  myGLCD.setFont(SmallFont);
  myGLCD.print("MINT LAB - Mg IMMERSION TEST", 50, 50);
  myGLCD.print("(c) yayoglu", 230, 225);

 }
```

78

APPENDIX D: COPYRIGHT PERMISSIONS

Below is the permission for the use of Figure 2.1.

<div style="border:1px solid #000; padding:10px;">

ELSEVIER LICENSE
TERMS AND CONDITIONS

Oct 18, 2016

This Agreement between Yahya E Yayoglu ("You") and Elsevier ("Elsevier") consists of your license details and the terms and conditions provided by Elsevier and Copyright Clearance Center.

License Number	3971720737429
License date	Oct 18, 2016
Licensed Content Publisher	Elsevier
Licensed Content Publication	Surface and Coatings Technology
Licensed Content Title	Corrosion behaviour of biodegradable magnesium alloys with hydroxyapatite coatings
Licensed Content Author	Conor F. Dunne,Galit Katarivas Levy,Orly Hakimi,Eli Aghion,Barry Twomey,Kenneth T. Stanton
Licensed Content Date	15 March 2016
Licensed Content Volume Number	289
Licensed Content Issue Number	n/a
Licensed Content Pages	8
Start Page	37
End Page	44
Type of Use	reuse in a thesis/dissertation
Portion	figures/tables/illustrations
Number of figures/tables/illustrations	1
Format	both print and electronic
Are you the author of this Elsevier article?	No
Will you be translating?	No
Order reference number	

</div>

Original figure numbers	Figure 10
Title of your thesis/dissertation	Corrosion Characteristics of Magnesium under Varying Surface Roughness Conditions
Expected completion date	Oct 2016
Estimated size (number of pages)	90
Elsevier VAT number	GB 494 6272 12
Requestor Location	Yahya E Yayoglu 14511 Prism Circle Apt 208 TAMPA, FL 33613 United States Attn: Yahya E Yayoglu
Total	0.00 USD

Below is the permission for the use of Figure 2.2.

ELSEVIER LICENSE
TERMS AND CONDITIONS

Oct 18, 2016

This Agreement between Yahya E Yayoglu ("You") and Elsevier ("Elsevier") consists of your license details and the terms and conditions provided by Elsevier and Copyright Clearance Center.

License Number	3971721085219
License date	Oct 18, 2016
Licensed Content Publisher	Elsevier
Licensed Content Publication	Corrosion Science
Licensed Content Title	Effect of heat treatment on corrosion behavior of AZ63 magnesium alloy in 3.5wt.% sodium chloride solution
Licensed Content Author	Jiarun Li,Quantong Jiang,Huyuan Sun,Yantao Li
Licensed Content Date	October 2016
Licensed Content Volume Number	111
Licensed Content Issue Number	n/a
Licensed Content Pages	14
Start Page	288
End Page	301
Type of Use	reuse in a thesis/dissertation

80

Intended publisher of new work	other	
Portion	figures/tables/illustrations	
Number of figures/tables/illustrations	1	
Format	both print and electronic	
Are you the author of this Elsevier article?	No	
Will you be translating?	No	
Order reference number		
Original figure numbers	Figure 4	
Title of your thesis/dissertation	Corrosion Characteristics of Magnesium under Varying Surface Roughness Conditions	
Expected completion date	Oct 2016	
Estimated size (number of pages)	90	
Elsevier VAT number	GB 494 6272 12	
Requestor Location	Yahya E Yayoglu 14511 Prism Circle Apt 208 TAMPA, FL 33613 United States Attn: Yahya E Yayoglu	
Total	0.00 USD	

Below is the permission for the use of Figure 2.3.

Licensed Content Author	Zhongwei Wang,Qing Li,Zuxin She,Funan Chen,Longqin Li,Xiaoxu Zhang,Peng Zhang
Licensed Content Date	15 April 2013
Licensed Content Volume Number	271
Licensed Content Issue Number	n/a
Licensed Content Pages	11
Start Page	182
End Page	192
Type of Use	reuse in a thesis/dissertation
Intended publisher of new work	other
Portion	figures/tables/illustrations
Number of figures/tables/illustrations	1
Format	both print and electronic
Are you the author of this Elsevier article?	No
Will you be translating?	No
Order reference number	
Original figure numbers	Scheme 3
Title of your thesis/dissertation	Corrosion Characteristics of Magnesium under Varying Surface Roughness Conditions
Expected completion date	Oct 2016
Estimated size (number of pages)	90
Elsevier VAT number	GB 494 6272 12
Requestor Location	Yahya E Yayoglu 14511 Prism Circle Apt 208 TAMPA, FL 33613 United States Attn: Yahya E Yayoglu
Total	0.00 USD

Below is the permission for the use of Figure 2.4 and Figure 2.5.

Below is the permission for the use of Figure 2.6.

**JOHN WILEY AND SONS LICENSE
TERMS AND CONDITIONS**

Oct 18, 2016

This Agreement between Yahya E Yayoglu ("You") and John Wiley and Sons ("John Wiley and Sons") consists of your license details and the terms and conditions provided by John Wiley and Sons and Copyright Clearance Center.

License Number	3971730172782
License date	Oct 18, 2016
Licensed Content Publisher	John Wiley and Sons
Licensed Content Publication	Advanced Engineering Materials
Licensed Content Title	On the Immersion Testing of Degradable Implant Materials in Simulated Body Fluid: Active pH Regulation Using CO2
Licensed Content Author	Michael Schinhammer,Joëlle Hofstetter,Christian Wegmann,Frank Moszner,Jörg F. Löffler,Peter J. Uggowitzer
Licensed Content Date	Jan 28, 2013
Licensed Content Pages	8
Type of use	Dissertation/Thesis
Requestor type	University/Academic
Format	Print and electronic
Portion	Figure/table
Number of figures/tables	1
Original Wiley figure/table number(s)	Figure 3
Will you be translating?	No
Title of your thesis / dissertation	Corrosion Characteristics of Magnesium under Varying Surface Roughness Conditions
Expected completion date	Oct 2016
Expected size (number of pages)	90

Requestor Location	Yahya E Yayoglu 14511 Prism Circle Apt 208 TAMPA, FL 33613 United States Attn: Yahya E Yayoglu
Publisher Tax ID	EU826007151
Billing Type	Invoice
Billing Address	Yahya E Yayoglu 14511 Prism Circle Apt 208 TAMPA, FL 33613 United States Attn: Yahya E Yayoglu
Total	0.00 USD

85